UILU-ENG 84-3606

Report No. 106

CRACK SHAPES DURING BIAXIAL FATIGUE

by

Ted A. Beer
Department of Mechanical and Industrial Engineering, UIUC

A Report of the
MATERIALS ENGINEERING - MECHANICAL BEHAVIOR
College of Engineering, University of Illinois at Urbana-Champaign
May 1984

ABSTRACT

Fatigue cracks from Inconel 718 specimens were incrementally sectioned to obtain estimates of crack profiles and aspect ratios. The specimens were tested to failure in strain control under three loading conditions: tension, torsion, and combined tension-torsion. A least squares fit ellipse was fit to the data from the cracks, giving a good estimate of the actual crack profile. For cracks which encountered an obstruction such as a grain boundary, the surface growth stopped, and growth was deeper into the specimen and the crack took on the shape of a rectangle.

Correlations between surface crack length and crack depth were found to be good for cracks with surface lengths in the range of 0.1 to 1.0 mm. Cracks from lower strain specimens have larger aspect ratios than cracks from high strain, low life fatigue specimens. The correlation suggests that for fatigue cracks from a specimen with equal strain amplitudes, tension, torsion, and combined tension-torsion cracks have very similar crack aspect ratios. For $\Delta\bar{\varepsilon}/2$ = 0.5 percent, the average aspect ratio given by maximum crack depth divided by surface crack length was 0.22. For $\Delta\bar{\varepsilon}/2$ = 1.0 percent, an average aspect ratio of 0.15 was found.

Observations of crack growth characteristics were also made, including crack bifurcation and the Stage I to Stage II transition.

Keywords: Biaxial fatigue, Small cracks, Crack growth, Aspect ratio

TABLE OF CONTENTS

LIST OF TABLES

LIST OF FIGURES

ACKNOWLEDGEMENTS

Professor Darrell F. Socie is gratefully acknowledged for his guidance and motivation throughout the investigation. Thanks are extended to Jon Pollack who faithfully assisted in the very tedious task of polishing the specimens.

Changtsan Hua is gratefully acknowledged for many stimulating discussions and assistance.

Financial support was provided by the Detroit Diesel Allison Division of General Motors and the Air Force Materials Laboratory under Contract F33615-81-C-5015.

1. INTRODUCTION

Modern systems such as aircraft, automobiles, and printing machines are growing more complex and operating at higher speeds than ever before. At the same time, constant pressure for cost effective designs demands optimization of each component; thus, the need for a reliable and consistently accurate method of design analysis is apparent. One important part of any dynamic design analysis is the consideration of the fatigue resistance. Fatigue occurs when components are subjected to repeated loading. In general, the loading is such that complex multiaxial states of stress occur. Unfortunately, data for the fatigue characteristics of materials are typically generated from uniaxial test programs. Because of the great complexity of biaxial loading, as well as the large number of tests required to develop empirical criteria, little research has been done on the multiaxial fatigue problem until recent years. Rather, research has centered on developing an appropriate rule which reduces the complex multiaxial loading to an "equivalent" uniaxial loading. Data from uniaxial tests can then be used to predict the fatigue resistance of components.

Several reviews of multiaxial fatigue are available [1,2], giving a broad background to the current state of the art. Recent approaches are based on the critical plane for crack initiation and growth. Two of the more popular approaches are those by Brown and Miller [3] and by Lohr and Ellison [4]. Both theories incorporate strain parameters which quantify the shear strain on the critical plane and the normal strain to that plane. Socie, et al. [5] has shown that both Brown and Miller and Lohr-Ellison parameters provided good correlation of the data and can be combined with uniaxial material properties to estimate lives in biaxial

loading. To further improve the life estimates of components subjected to multiaxial loading, a better understanding of the mechanism of crack growth must be obtained.

This investigation centers on the relationship between the length of a crack on the surface of a component and the depth of that crack. The ratio of crack depth to surface length is known as the aspect ratio. The greater the crack depth, the greater the damage. The material used in this investigation was taken from the gage section of thin-walled tubes of Inconel 718. Surface crack observations for this material have been made by Waill [6]. The specimens were subjected to in-phase, room temperature, biaxial, strain controlled tests. Cracks which developed as a result of this loading were sectioned from 5 to 15 times and the depth of the crack was measured at each interval. Crack profiles from approximately 90 cracks were determined by this method. Correlations between surface crack length and maximum crack depth were determined.

Additionally, observations were made on the growth of cracks into the sample. These observations included crack bifurcation and its causes and, in the language of Forsyth [7], Stage I and Stage II transition of crack growth planes.

2. EXPERIMENTAL PROCEDURE

2.1 Material

Specimens were cut from a forged ring of Inconel 718 purchased to Aerospace Material Specification, AMS 5663. Inconel 718 is a high temperature, nickle based superalloy. The ring (800 mm OD, 650 mm ID) was sectioned into 75 mm x 75 mm x 225 mm blocks with the long dimension parallel to the axis of the ring. The microstructure is shown in Fig. 1. A mixture of grain sizes was observed ranging from small clusters where the typical diameter was 0.01 mm to areas with grains as large as 0.2 mm. These are at least 10 grains through the specimen thickness for the largest grains. Residual stresses induced during forging were relieved after rough machining by heat-treatment at 600°C for twelve hours, which prevented the specimen from distorting during final machining. Tensile properties are given in Table 1.

2.2 Sectioning Procedure

Fatigue cracks were sectioned from specimens tested under biaxial loading conditions. Tests to failure on the Inconel specimens were conducted for axial ($\lambda = 0$), torsional ($\lambda = \infty$), and combined tension-torsion loading ($\lambda = \sqrt{3}$) where λ is the ratio of torsion to tensile strain amplitude. For each of the above loading modes, one series of tests was conducted at a strain ratio of $R_\varepsilon = -1$ and a second series at $R_\varepsilon = 0$ where R_ε is the ratio of minimum to maximum strain. The tests at each strain ratio were conducted at two effective strain amplitudes, $\Delta\bar{\varepsilon}/2 = 0.5$ percent and 1.0 percent. In all, a total of twelve specimens were prepared for this investigation. Table 2 shows the fatigue results for the ten specimens which provided crack depth data.

Failed specimens contained a large number of cracks with a wide range of surface crack lengths. As a result, crack shape as a function of length could be obtained from a single specimen.

The general procedure followed in determining a crack profile consisted of the following steps. A crack of the desired surface length was located on the specimen. The length was accurately measured using the calibrated eyepiece of an optical microscope. The specimen surface perpendicular to the surface crack was ground away until approximately one-tenth of the crack length was removed, which exposed the crack growing into the depth of the specimen. Using standard metallographic specimen polishing techniques, the ground surface was polished carefully to reveal the crack. The new surface crack length was measured, then the specimen was rotated 90° and the depth of the crack measured. This procedure was repeated until the surface crack was completely eliminated.

In light of the large number of cracks being investigated, it was necessary to design a fixture to hold the specimen in such a way that several cracks could be sectioned at the same time. It was also necessary to design the fixture to accommodate the various crack directions obtained from the three loading modes. In torsion, cracks grow principally on the longitudinal specimen axis. Tension cracks tend to grow in a circumferential direction, and the combined tension-torsion cracks grow at an intermediate angle, usually 20 or 70 degrees from the longitudinal axis. Only the tension and torsion cracks were sectioned in a direction perpendicular to the surface crack. Combined loading cracks were sectioned at an angle of 20 degrees from the surface crack direction. Because of this sectioning angle, care must be taken in interpreting the direction of the crack growing into the depth of the

specimen loaded in combined tension-torsion. In addition, because of the small dimensions of the cracks, it was necessary to precisely machine the fixture in order to ensure that the measured crack depth corresponded to the surface crack being investigated.

The fixture used when studying torsion or combined tension-torsion is shown in Fig. 2. Figure 2a shows the fixture as it would appear when measuring the surface crack length. Figure 2b shows the fixture rotated 90 degrees to allow measurement of the crack depth. Figure 3 shows the fixture used to accommodate tension samples.

3. RESULTS

Numerical results of depth measurements from crack sectioning are given in the APPENDIX in Tables A.1 to A.10. Specimen identification is given in Table 2. Each table lists the data for eight to ten cracks from a single specimen. The total length for each crack is given as 2c, and the depth of the crack a at locations L along the crack is given at several intervals. The numerical results are given for strain amplitudes of 1.0 percent and 0.5 percent at strain ratios R_ε = -1 and 0 for both the torsion and the combined tension-torsion specimens, for a total of eight specimens. For the tension samples, however, crack sectioning could only be carried out at the 0.5 percent strain amplitude. At the higher strain amplitude of 1.0 percent, the surface was characterized by many very short cracks and a single large failure crack. Since very few intermediate cracks were present on the samples loaded at the higher strain amplitude, it was not feasible to section them. Figure 4 shows typical surface topography for 1.0 percent strain amplitude tensile loading at R_ε = -1 and 0. These surfaces are typical of high strain amplitude axial loading [6].

Figures 5 through 14 are two-dimensional graphical representations of crack profiles for each crack sectioned. Each figure shows six to eight cracks from a single specimen, providing a range of profiles for surface crack lengths of 0.2 to 1.0 mm.

As a means of modeling each crack, a least squares fit ellipse of the form

$$\frac{x^2}{c^2} + \frac{y^2}{a^2} = 1 \qquad (1)$$

is shown to fit the data points. An ellipse was chosen as the mathematical model of the cracks for several reasons. First, in linear elastic fracture mechanics, cracks have typically been represented as ellipses. Parameters such as the flaw shape parameter have often been derived in terms of the ellipse and, more importantly for most of the cracks sectioned, the experimental data fit the elliptical shape well. Torsion cracks fit the elliptical shape better than either the combined tension-torsion or the tension cracks.

It was assumed that the surface crack length was known to have a greater degree of accuracy than were the depth measurements. Using this assumption, Eq. (1) was treated as if error were only introduced in the depth measurements. The parameter a is then the only variable which needs to be considered in the least squares formulation. In this case, a is the minor axis of the ellipse and, therefore, can be used as the maximum crack depth. By using a consistent model for determining the crack depth, the arbitrary choice of a maximum crack depth is eliminated. In most cases, the maximum crack depth obtained experimentally is very close to that predicted by the elliptical model. Maximum crack depth a is given by:

$$a = \frac{\sum_{i=1}^{n} y_i [1 - (x_i/c)^2]^{1/2}}{\sum_{i=1}^{n} (1 - (\frac{x_i}{c})^2)}, \qquad (2)$$

where n is the number of sectioning intervals, y_i is the depth of the crack at the i^{th} interval, x_i is the distance from the center of the crack to the sectioning location, and c is one-half the total crack length.

Correlations between surface crack length and crack depth can be made from data such as that collected in this experiment. Figures 15 through 20 are plots of maximum crack depth a versus surface crack length 2c. Each figure compares the crack depth and surface crack length for different loading conditions. A least squares linear fit of the data has been made and fits the data well.

4. DISCUSSION

4.1 Preliminary Remarks

Before beginning a discussion of the specific results applying to the aspect ratio correlations found experimentally, a general discussion of the cracking behavior will be given.

In performing crack depth measurements using an optical microscope, the tip of the crack must be clearly defined to ensure accurate measurement. In many cases however, the cracks were not visible; in combined tension-torsion and tension cracks where there is a component of Mode I crack opening, the cracks close when unloaded and appear to have healed. Without some additional means of revealing the crack tip, accurate depth measurements would be impossible. Torsional cracks, whose surfaces tend to rub over each other as a result of Mode II crack opening, are usually readily visible all the way to the crack tip. To heighten the visibility of those cracks which were tightly closed, each sample was plastically deformed in such a way as to open the crack. The method of deformation consisted of three-point bending. To avoid the possibility of actually extending the crack as a result of the plastic deformation, the bending was carried out in a series of steps. The applied load was steadily increased at each step while monitoring the crack tip position. It was found that for this material, a very large stress was necessary to cause crack extension. In addition, a zone of plastic deformation was visible at the crack tip before the extension occurred, giving warning that too large a stress was applied. This method provides easily measureable crack depths. In developing the crack in this manner, the experimenter can be confident in the depth measurement. Care must be taken to limit the stressing of the samples as much as possible if many cracks are to be sectioned.

It is important to note the range of the surface crack lengths being studied. The cracks measured in this experiment ranged from 0.1 to 1.0 mm. Much of the data taken on crack aspect ratios in the past have been for cracks greater than 1.0 mm in length, typically in the range of 1.5 mm [8,9]. Socie, et al. [5] have shown that for this material, 75 to 95 percent of the component life in tension and combined tension-torsion and 50 to 70 percent of component life in torsion is spent growing cracks to a length of 1.0 mm. At crack lengths greater than 1.0 mm, growth occurs at a much greater rate and the cracks became large with respect to the dimensions of the specimen. With such a large percentage of the component life spent growing cracks to 1.0 mm, a better understanding of their growth characteristics is important.

When determining the aspect ratio of a crack, most investigators have assumed that the crack depth reaches a maximum at the midpoint of the crack [7,9]. Careful examination of Figs. 5 through 14 shows that this is often not the case. Instead, the cracks sometimes tend to grow deepest near one end. This trend results in a crack shape more closely approximating a rectangle than an ellipse.

When a crack growing along the surface of a specimen encounters an obstruction such as a grain boundary, its growth is impeded. Figure 21 shows a combined tension-torsion crack intersecting an obstruction. Its growth on the surface has been stopped. Upon sectioning this crack, it was found that the maximum depth remained constant to the end of the crack. Thus, when the surface growth of a crack is impeded, the crack grows into the depth.

This result is especially important when considering the sectioning results for short cracks, in the range of 0.1 to 0.2 mm. The crack pro-

file figures demonstrate that in nearly every case, cracks in this range were rectangular in shape and had an aspect ratio much greater than the expected value. Recall that the grain size of this material is 0.1 to 0.2 mm. At specimen failure, it was very difficult to find a crack of 0.1 mm which had not had its surface length impeded. Differences in material purity and grain structure in materials could certainly cause the variation in aspect ratios which have been reported. Dowling [8] eliminated this problem by stopping the test when the surface crack grew to the desired length, rather than taking the specimen to failure. The specimen was cracked open to reveal the entire crack profile. The method would assist in determining an accurate crack profile for cracks of any length for a wider range of strain levels.

An alternate method would be to examine cracks located on the radius of the specimens, rather than in the gage section. Because of the greater wall thickness, the applied stress is lower and cracks in these locations would also tend to accurately reflect the correct crack profile for a wider range of strain levels. Both of the above methods would be inefficient for collecting the large amounts of data necessary to make accurate statistical correlations.

Finally, when comparing data for crack aspect ratios, it is important to note the lives to failure of the specimen. As will be discussed later, the aspect ratio increases as the strain amplitude decreases. Thus, lower strain, tests have a greater aspect ratio than high strain low life tests. The majority of experimental results thus far have been obtained from specimens with failure lives of 10^5 to 10^6 cycles [8,9]. The values reported have typically been higher than those reported in this paper, which were taken from specimens with lives of 103 and 104 cycles.

4.2 Aspect Ratio Correlations

Data from crack depth measurements suggest that correlations between surface crack length and crack depth can be made for cracks in the range of 0.1 to 1.0 mm. Figure 15 shows the crack depth, a, computed from Eq. (2) versus crack length, 2c, data for $R_\varepsilon = 0$, $\Delta\bar{\varepsilon}/2 =$ 0.5 percent strain amplitude loading conditions. Tension, torsion, and combined tension-torsion data are each plotted on the graph. A least squares fit to the data is shown as the solid line. The most readily apparent result from the data is that all three loading modes have equal aspect ratios. The solid line fits all three sets of data with minimal scatter. The aspect ratio a/2c for the specimen is 0.22. Some investigators have found that the aspect ratios for tension are greater than that of torsion, with values for combined loading lying between the two. These aspect ratios also tend to be higher, with values up to 0.5 reported for tension. It is suggested that these differences are due to the use of longer crack lengths and longer failure lives of the specimen being studied by the earlier workers. This follows what was explained earlier in the discussion. Note also that the majority of the work done to date has been on medium carbon and low alloy steels. These steels tend to have greater amounts of inclusions and defects than the Inconel used in this test. Material differences would certainly create different crack growth conditions. This result suggests that for short cracks in Inconel, growth rates into the specimen are similar to the surface growth rate for the three loading modes investigated. Note that as surface length increases, the scatter in all of the data increases. Also, the combined loading specimens had more scatter than the tension or torsion specimens.

Figure 16 shows a versus 2c data for the $R_\varepsilon = -1$, $\Delta\bar{\varepsilon}/2 =$ 0.5 percent strain amplitude loading conditions. Again, tension, torsion, and combined loading data are plotted on the graph. Here it is seen that the tension and torsion data fit the same least squares line very closely, but unlike the $R_\varepsilon = 0$ loading mode, the combined loading has a lower aspect ratio. The value for the tension and torsion samples is 0.32, while that of the combined loading is given as 0.22. Note that again, like the $R_\varepsilon = 0$ loading mode, the combined loading specimen data showed more scatter than either tension or torsion. An accurate relationship between a and 2c for combined loading is difficult to characterize because of scatter in the data. Close observations of the a versus 2c data for the combined loading specimen in this figure might suggest a better correlation. Notice that a horizontal line at a = 0.12 accurately describes the relationship between depth and surface length. It is also seen that this trend is visible in Specimen B-16, a torsional specimen at a strain amplitude of 1.0 percent. In the author's opinion, more data from these specimens must be collected before an accurate correlation can be made.

Figures 17 and 18 show the a versus 2c data for the $R_\varepsilon = -1$ and 0 strain ratios at a strain amplitude of 1.0 percent. Torsion and combined tension-torsion data are shown, with no 1.0 percent amplitude tension data available. A similar trend to that seen above in the low strain amplitude data is observed. For $R_\varepsilon = -1$, both sets of data lie along a line corresponding to an aspect ratio of 0.14. For $R_\varepsilon = 0$, a least squares line fits the data well, but gives a slightly higher aspect ratio of 0.17. It is observed, however, that there is a significant divergence in the data past a crack length of 0.8 mm. If these

cracks are removed from the plot, or data are plotted only for cracks in the range of 0.1 to 0.8 mm, the data very closely matches the aspect ratio of 0.14 found in the $R_\varepsilon = -1$ data.

If crack lengths up to 0.8 mm are plotted, a reasonably good correlation can be made for the six loading modes considered in this study. Figure 19 shows all of the data points collected for the 0.5 percent strain amplitude tests for surface crack lengths up to 0.8 mm. It is seen that the data fit a least squares line corresponding to an aspect ratio of 0.22.

Figure 20 is a collection of all data points collected for the 1.0 percent strain amplitude tests for surface cracks up to 0.8 mm. For these data points, a least squares line corresponding to an aspect ratio of 0.15 fits the data well.

From the plots above, it is further clarified that the variations in the aspect ratios for tension, torsion, and combined tension-torsion are small for the range of crack sizes being considered. They also accentuate the trend that smaller strain amplitude tests provide larger aspect ratios. It must be remembered that this is a correlation between surface crack length and crack depth. Although the low strain amplitude tests have a greater aspect ratio, the high strain amplitude specimens may fail sooner because of the greater growth rate of surface cracks at high amplitudes.

4.3 Depth Crack Observations

Figures 22 through 30 show actual crack profiles for each of the specimens investigated. The upper photograph shows the particular surface crack being investigated before sectioning. These cracks are on

the maximum shear strain planes. The lower photograph is a composite of several photographs, each showing the crack depth at a different location along the surface crack. The individual pictures were made each time the crack was metalographically sectioned. A good representation of the actual crack profile is given by the composite photographs in the figures. The typical shapes of depth cracks in each of the three loading modes can be seen in the figures.

Figures 22 through 25 show torsion cracks from various loading modes. Depth cracks into torsional specimens always grew radially inward along a plane of maximum shear. A very small amount of deviation in the crack direction occurred as it encountered changing grain structure. A phenomenon observed in a large number of torsional cracks was bifurcation. Crack bifurcation occurs when a single primary crack branches, forming two secondary cracks. The bifurcation process can occur several times on a single crack. An example of crack bifurcation in torsional cracks is seen in Fig. 31. Crack branching did not appear to be dependent upon crack depth, but occurred at many depths. Figures 31 and 32 show etched torsional specimens. The etchant reveals the interaction of the crack with the grain structure of the material. In the majority of cases, crack bifurcation occurred at the grain boundary. The crack grew along the grain boundary, then switched to transgranular growth. An example is given in Fig. 33. Figure 31 shows one of the few times when bifurcation did not occur at the grain boundary intersection, but within a grain. Note that the bifurcation direction coincides with the direction of the slip lines within the grains.

Figures 26 through 28 show combined tension-torsion crack profiles from various loading modes. The cracks in combined loading usually in-

itiates radially and grows inward toward the center of the specimen. However, unlike the torsional cracks, combined loading cracks tend to wander to a greater extent, seeming to follow the slip lines of the grains encountered. Crack growth in combined loading tends to be primarily transgranular. Figure 24 shows an etched combined loading specimen which illustrates the above observations. Crack bifurcation also occurs in combined loading specimens, but to a lesser degree. In general, a single main crack forms and remains dominant. Note that for the combined loading specimen, cracks were sectioned at approximately a 20 degree angle to the surface crack. The directions of the depth cracks shown in the above photographs are not principal planes, but they give a good idea of the nature of the combined loading crack.

Figures 27 and 30 show tension crack profiles for two loading modes. For tension cracks, initiation and early propagation occurs on maximum shear strain planes both on and into the surface of the specimen. Then, after two or three grain diameters, propagation direction into the surface changes to the principal strain plane. On the specimen surface, the crack remains on maximum shear strain planes for a longer period of time. This is the Stage I and to Stage II transition observed by Forsyth [7]. Figure 35 shows examples typical of Stage I to Stage II transition. Figure 36 shows two tensile cracks from an etched specimen. It is seen that crack propagation is transgranular, with Stage I to Stage II transition occurring at a grain boundary. Transition occured at a variety of crack depths. Bifurcation also occurs in tensile cracks, but to a much lesser degree than in the torsion specimens. It was always observed to occur at a grain boundary. Figure 37 shows a tensile crack in a etched specimen. Note the way the longer crack

follows the slip lines of the grains encountered. The smaller crack below shows a bifurcated crack.

5. CONCLUSIONS

1. Crack profiles for tension, torsion, and combined tension-torsion loading modes can be modeled with good accuracy by an ellipse.
2. Upon encountering an obstruction such as a grain boundary, a crack may stop propagating on the surface and grow into the specimen. The crack profile for this case is then more closely approximated by a rectangle rather than an ellipse.
3. Good correlations between surface crack length and crack depth can be made in the range of 0.1 to 1.0 mm surface lengths for Inconel 718.
4. Cracks from low strain, long life fatigue specimens have larger aspect ratios than cracks from high strain, low life fatigue specimens.
5. At a constant strain amplitude, tension, torsion, and combined tension-torsion specimens have crack aspect ratios which are very similar. For $\Delta\bar{\varepsilon}/2 = 0.5$ percent, an average value of $C/2a = 0.22$ has been found. For $\Delta\bar{\varepsilon}/2 = 1.0$ percent, an average value of $C/2a = 0.15$ is found. These values apply to a crack range from 0.1 to 0.8 mm surface lengths.

Table 1 Mechanical Properties

Monotonic Properties

Modulus 209 GPa	
Yield stress 0.2 percent	1160 MPa
Fracture stress	1850 MPa
Fracture strain	0.33
Percent Reduction in Area	28
Strength coefficient	1910 MPa
Strain Hardening Exponent	0.08

Cyclic Properties

Fatigue Strength Coefficient	1640 MPa
Fatigue Strength Exponent	-0.06
Fatigue Ductility Coefficient	2.67
Fatigue Ductility Exponent	-0.82
Cyclic Strength Coefficient	1530 MPa
Cyclic Strain Hardening Exponent	0.07

Table 2 Fatigue Test Results

Specimen	Nominal Strain Amplitude We/2	Wq/2	Nominal Stress Amplitude Ws/2(MPa)	Wt/2(MPa)	Mean Stress s_o(MPa)	t_o(MPa)	Fatigue Life $N_{0.1}$	$N_{1,0}$	N_f
Torsion									
R_e = 0									
B-32	0	0.0085	0	500	0	70	500	4500	9526
B-16	0	0.017	0	560	0	10	200	800	1738
R_e = -1									
B-8	0	0.0085	0	510	0	0	2000	7000	12942
B-13	0	0.17	0	570	0	0	100	800	1674
Combined									
R_e = 0									
B-34	0.0035		0.0063	610	380	170	30	2200	4800	5963
B-10	0.007		0.012	740	710	0	10	200	1000	1502
R_e = -1									
B-26	0.0035		0.0063	630	375	0	0	2000	8000	12899
B-11	0.007		0.12	740	410	0	0	300	1200	1581
Axial									
R_e = 0									
B-15	0.005		0	930	0	210	0	1500	6000	8000
R_e = -1									
B-12	0.005		0	920	0	0	0	2000	11000	13364

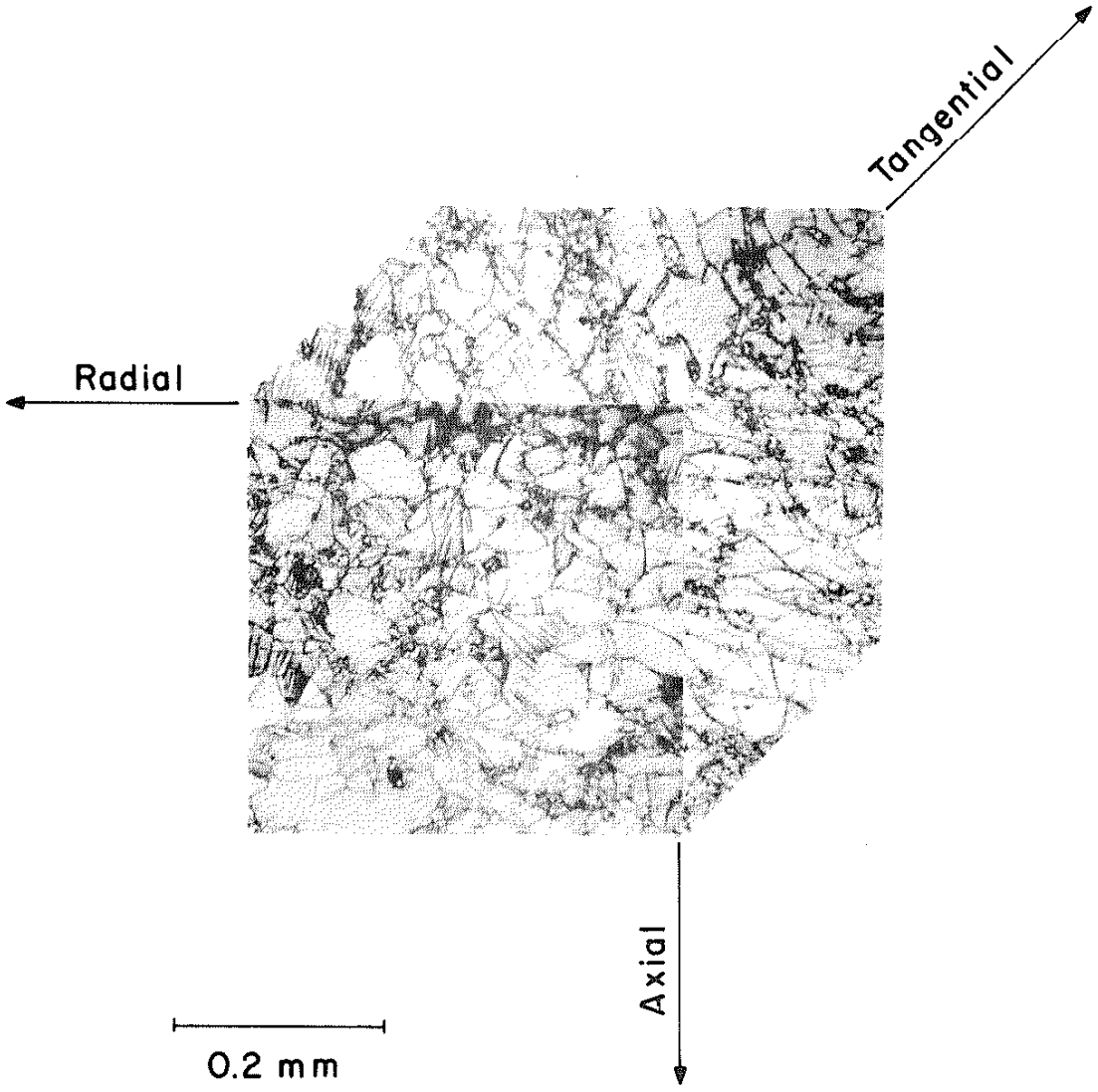

Figure 1 Grain structure

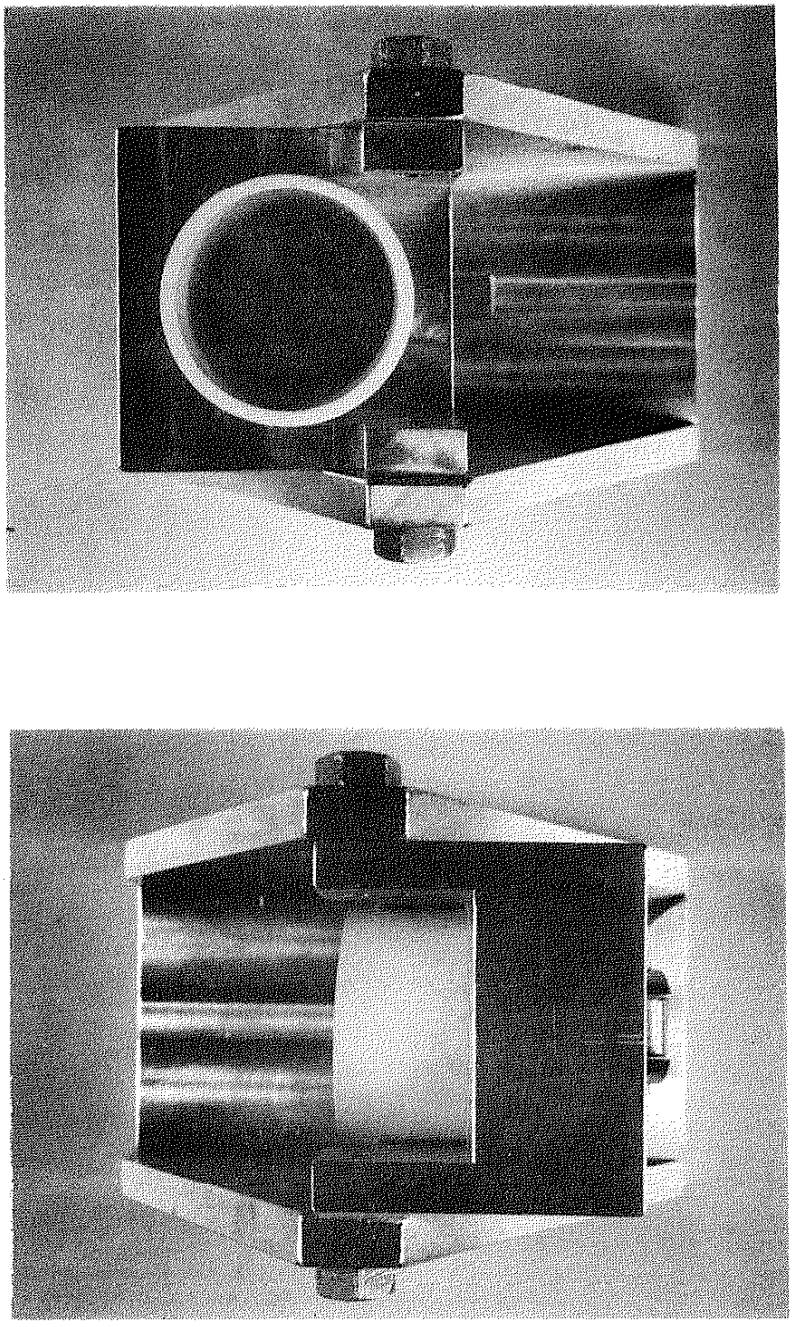

Figure 2 Test fixture for torsion and combined loading specimens

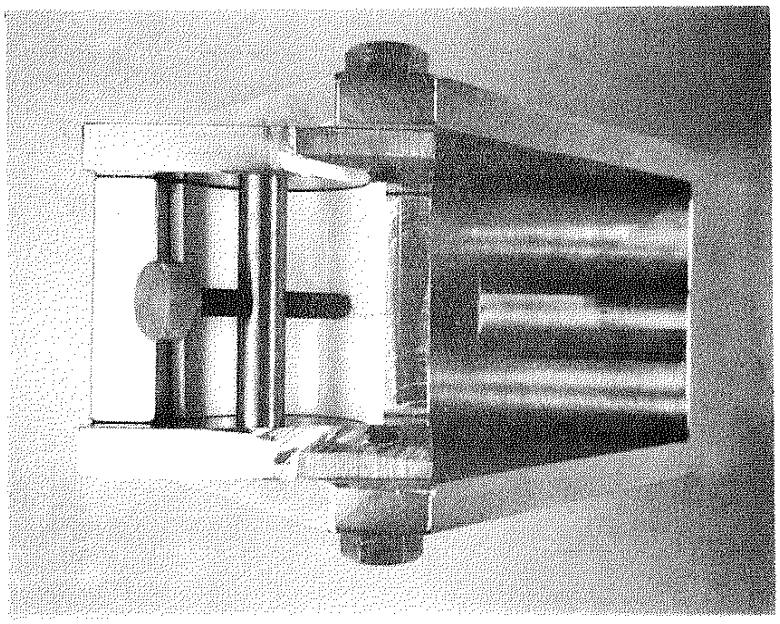

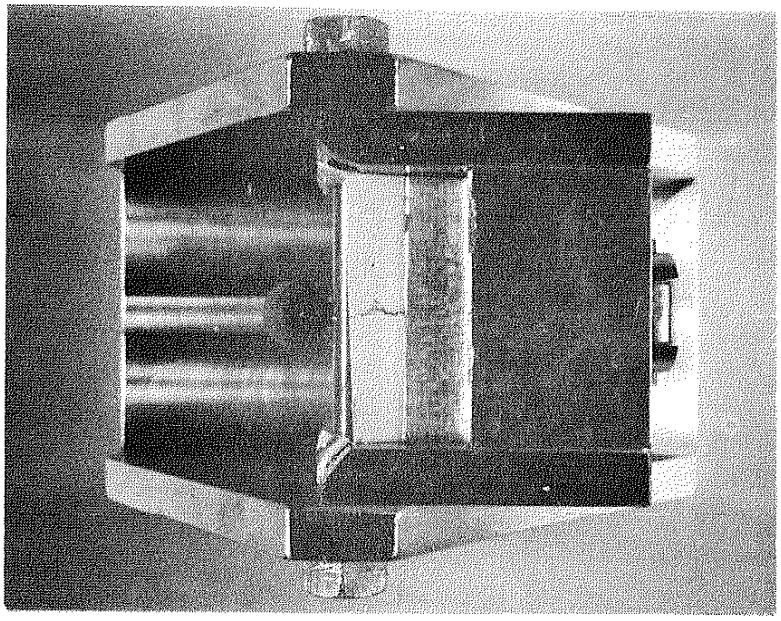

Figure 3 Test fixture for tension loading specimens

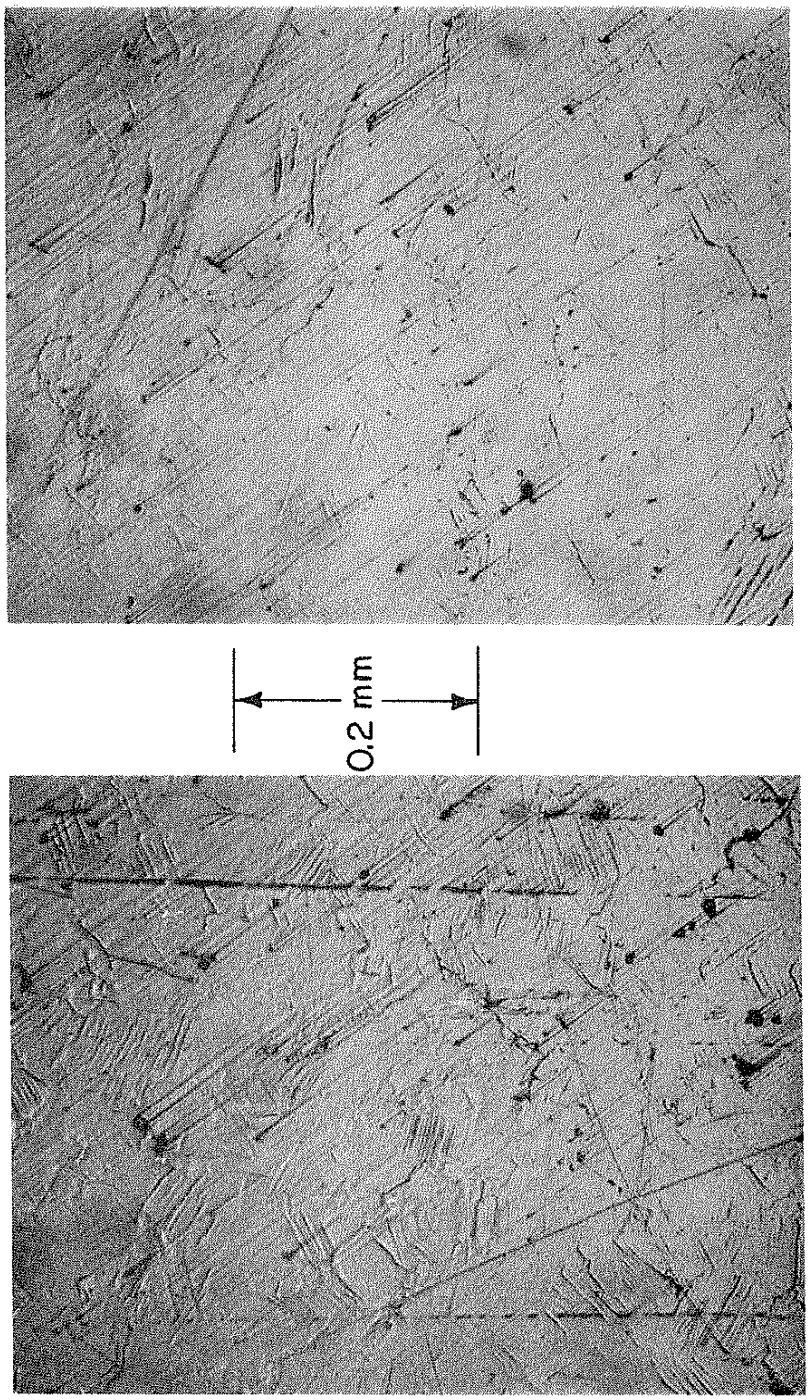

Figure 4 Typical surface topography for $\Delta\bar{\varepsilon}/2$ = 1.0% tension samples

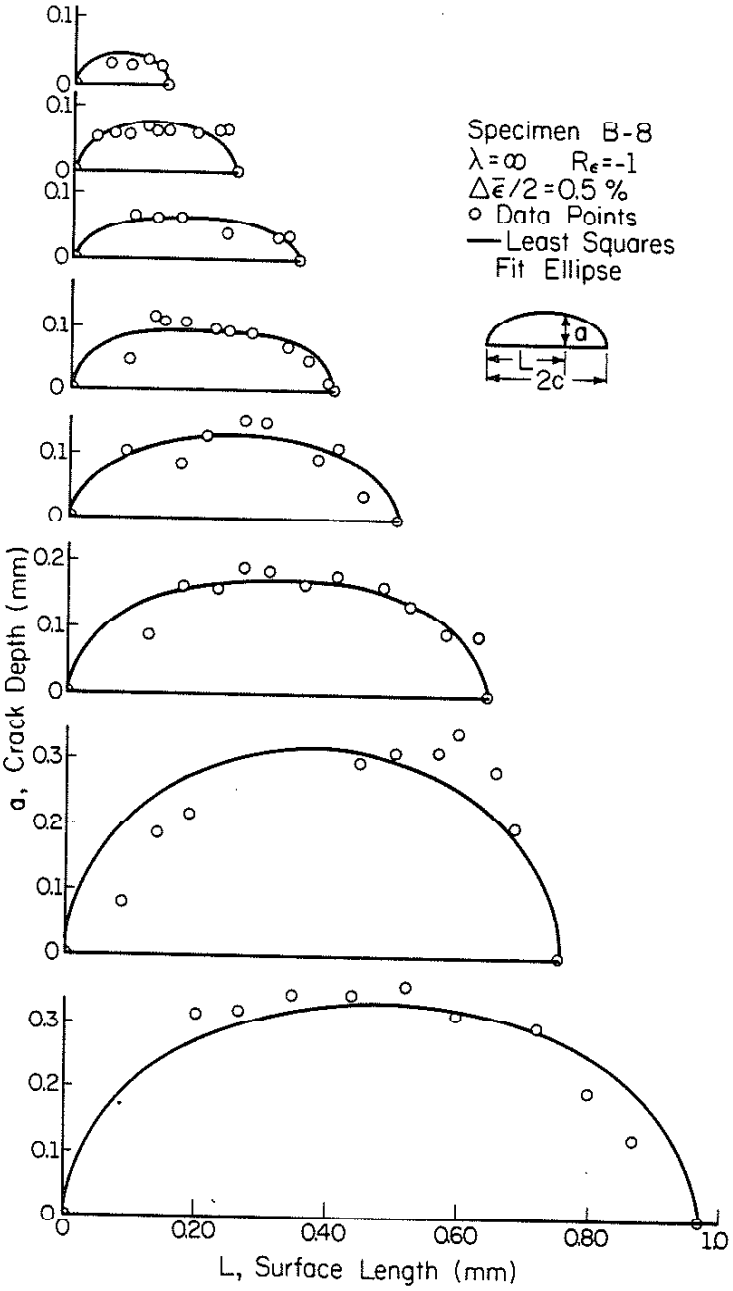

Figure 5 Least squares fit ellipse crack profiles, $\lambda = \infty$, $\Delta\bar{\varepsilon}/2 = 0.5$ percent, $R_\varepsilon = -1$

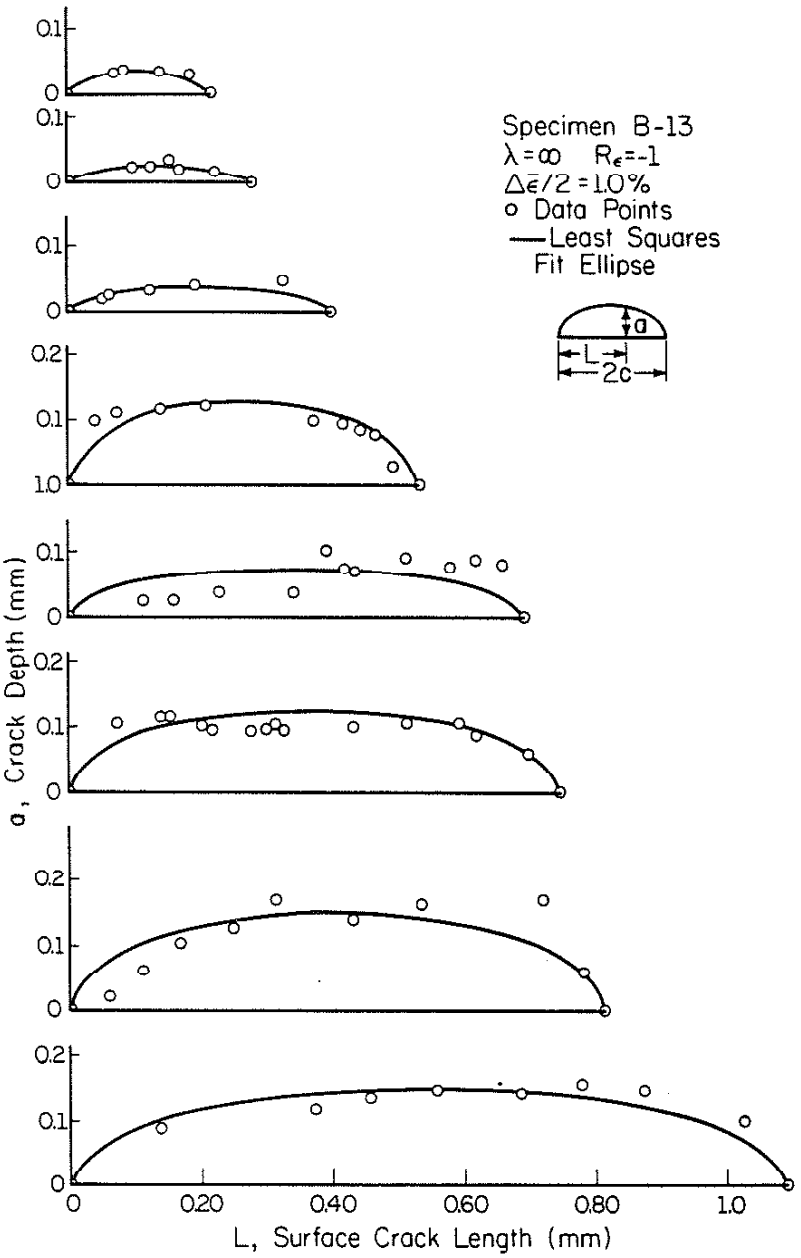

Figure 6 Least squares fit ellipse crack profiles, $\lambda = \infty$, $\Delta\bar{\epsilon}/2 = 1.0$ percent, $R_\epsilon = -1$

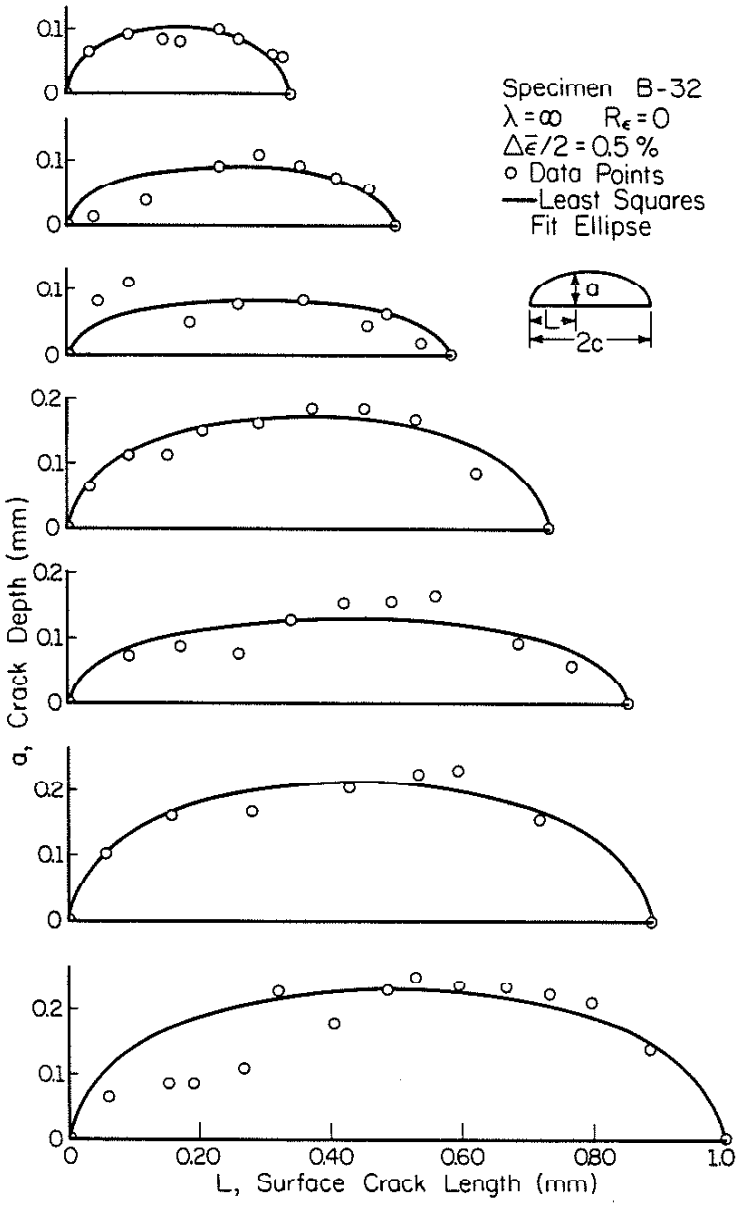

Figure 7 Least squares fit ellipse crack profiles, $\lambda = \infty$, $\Delta\bar{\varepsilon} = 0.5$ percent, $R_\varepsilon = 0$

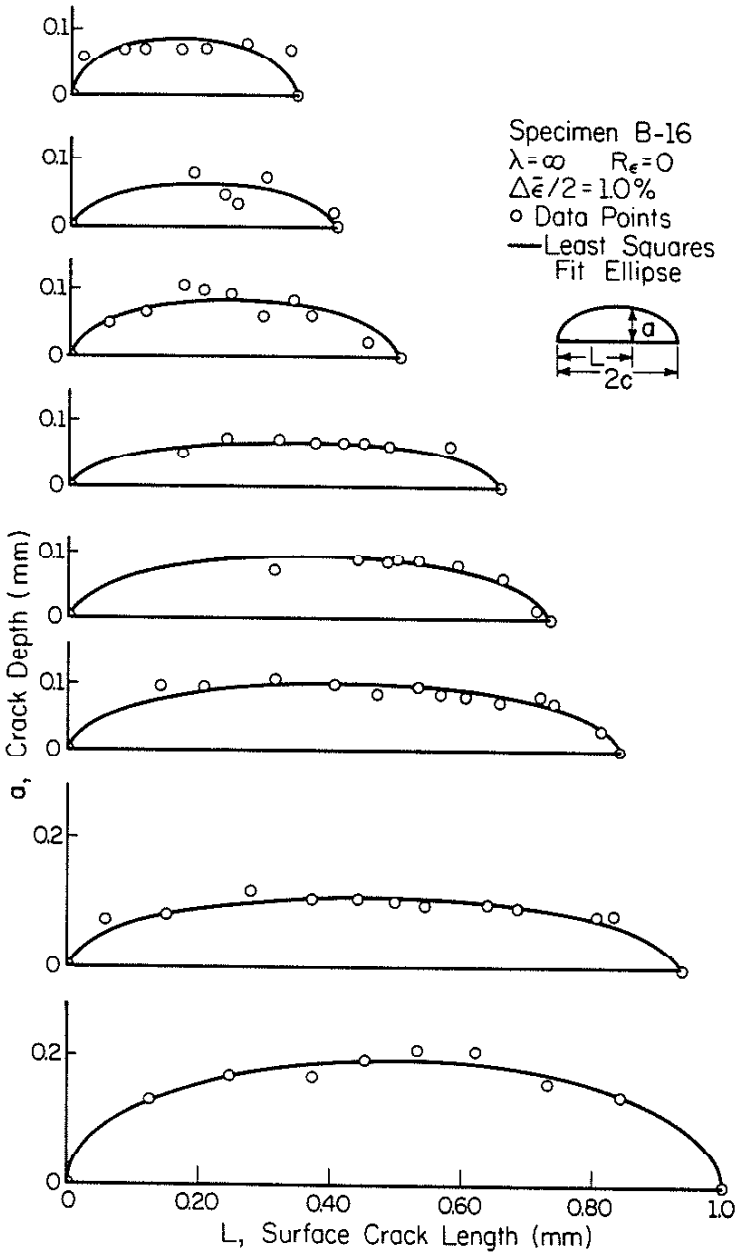

Figure 8 Least squares fit ellipse crack profiles, $\lambda = \infty$, $\Delta\bar{\varepsilon} = 1.0$ percent, $R_{\varepsilon} = 0$

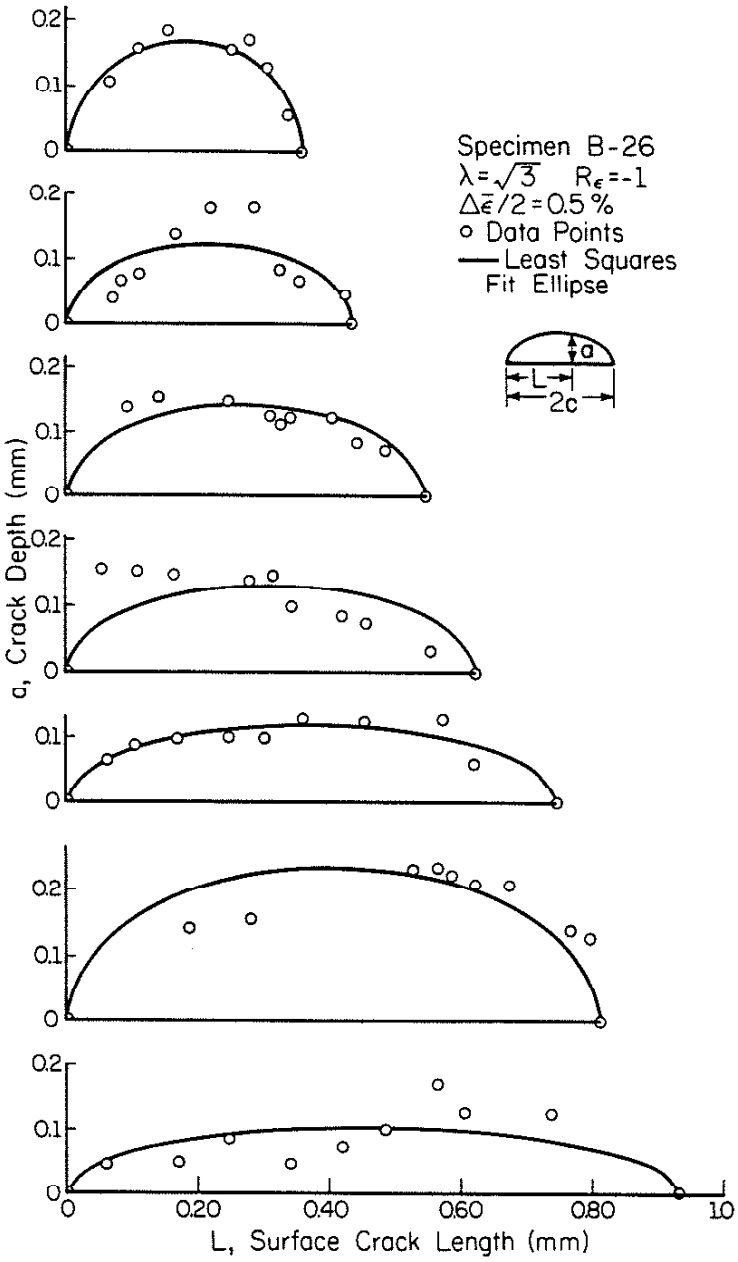

Figure 9 Least squares fit ellipse crack profiles, $\lambda = \sqrt{3}$, $\Delta\bar{\varepsilon}/2 = 0.5$ percent, $R_\varepsilon = -1$

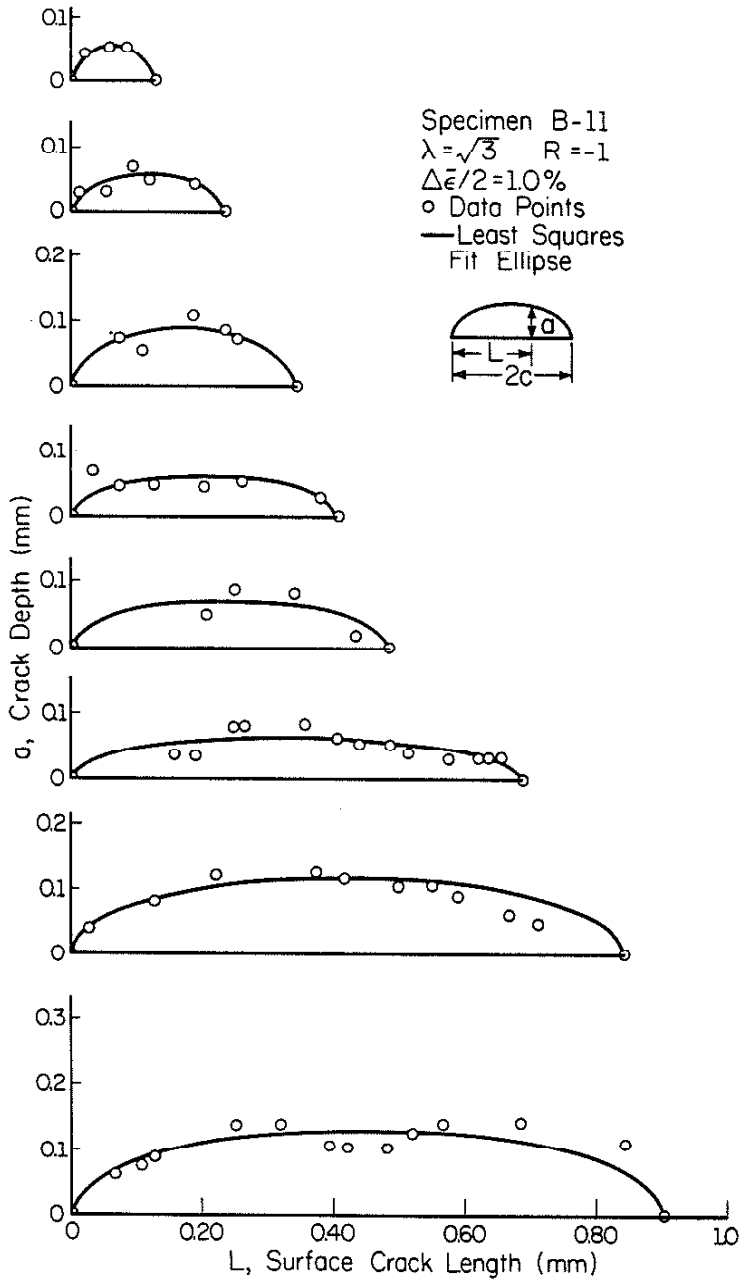

Figure 10 Least squares fit ellipse crack profiles, $\lambda = \sqrt{3}$, $\Delta\bar{\varepsilon}/2$, 1.0 percent, $R_\varepsilon = -1$

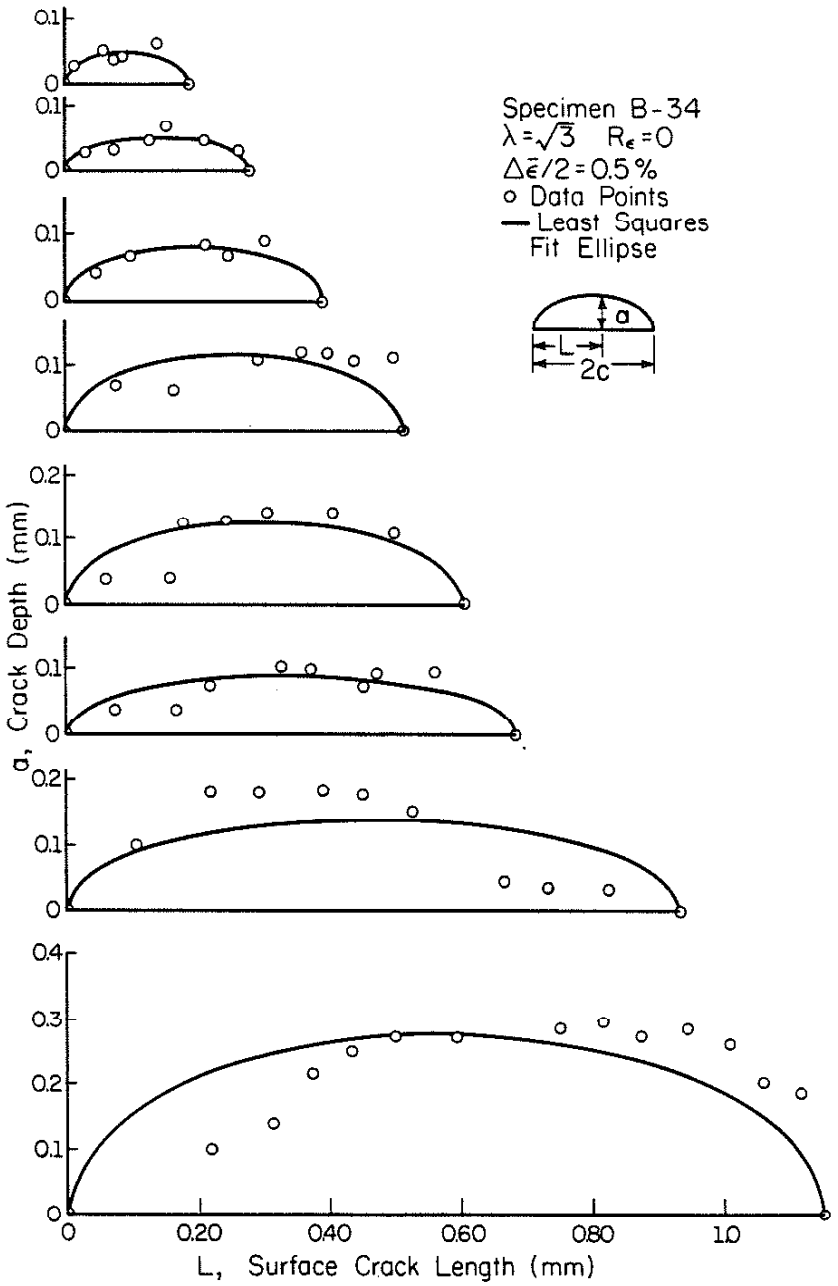

Figure 11 Least squares fit ellipse crack profiles, $\lambda = \sqrt{3}$, $\Delta\bar{\varepsilon}/2 = 0.5$ percent, $R_\varepsilon = 0$

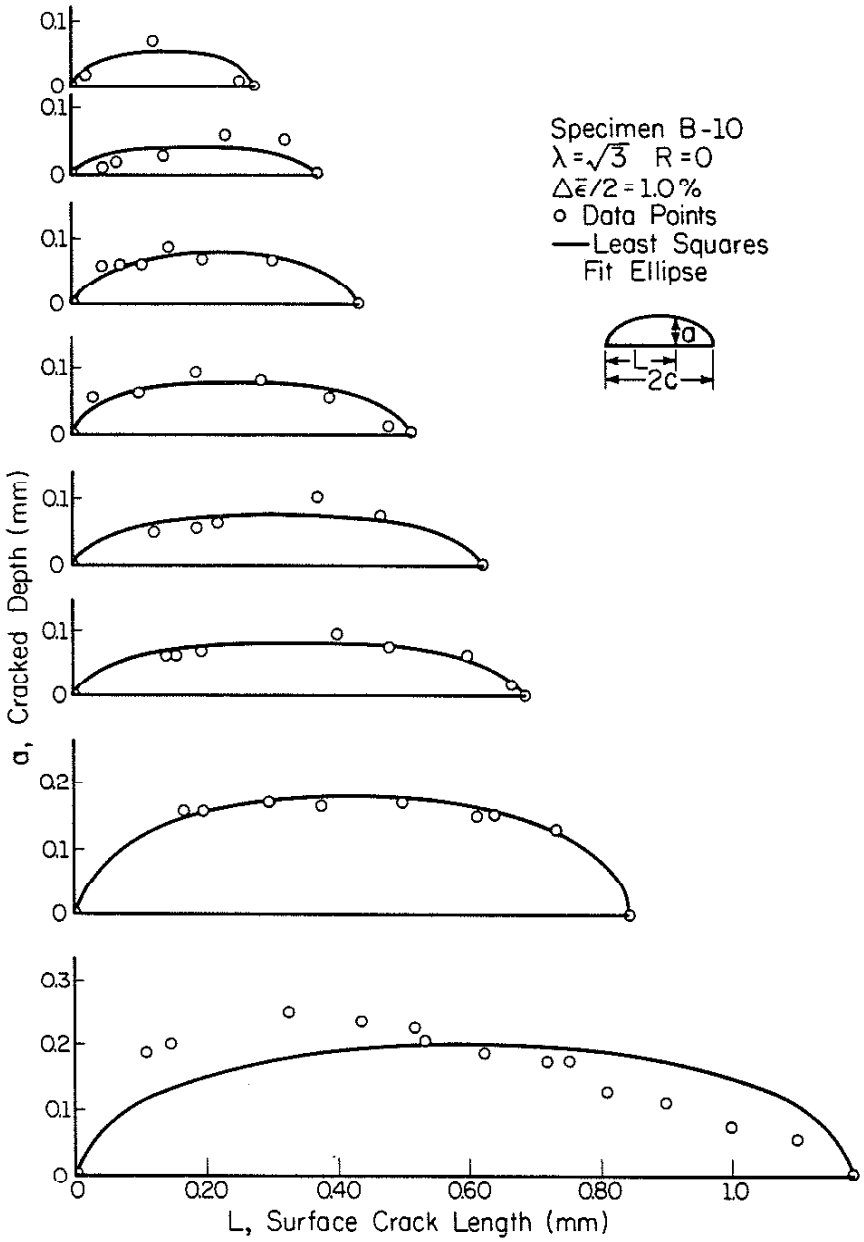

Figure 12 Least squares fit ellipse crack profiles, $\lambda = \sqrt{3}$, $\Delta\bar{\varepsilon}/2 = 1.0$ percent, $R_\varepsilon = 0$

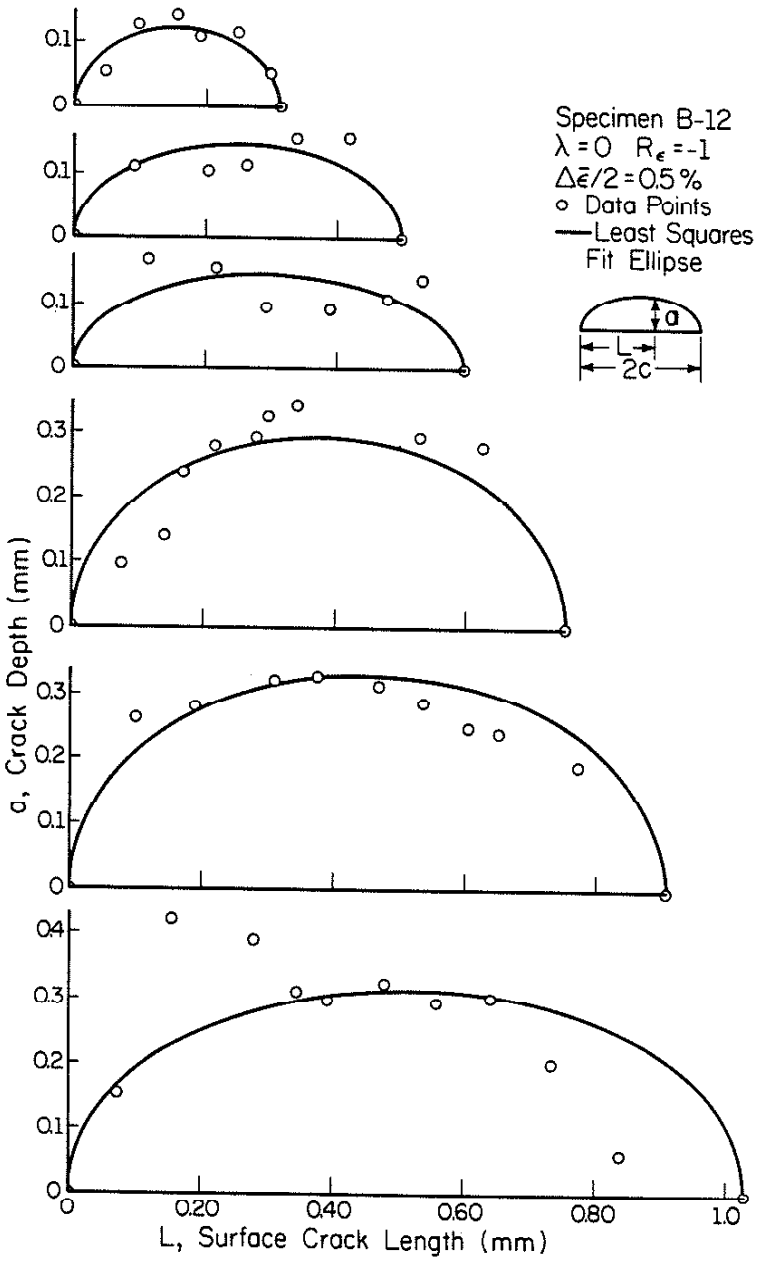

Figure 13 Least squares fit ellipse crack profiles, $\lambda = 0$, $\Delta\bar{\varepsilon}/2 = 0.5$ percent, $R_\varepsilon = -1$

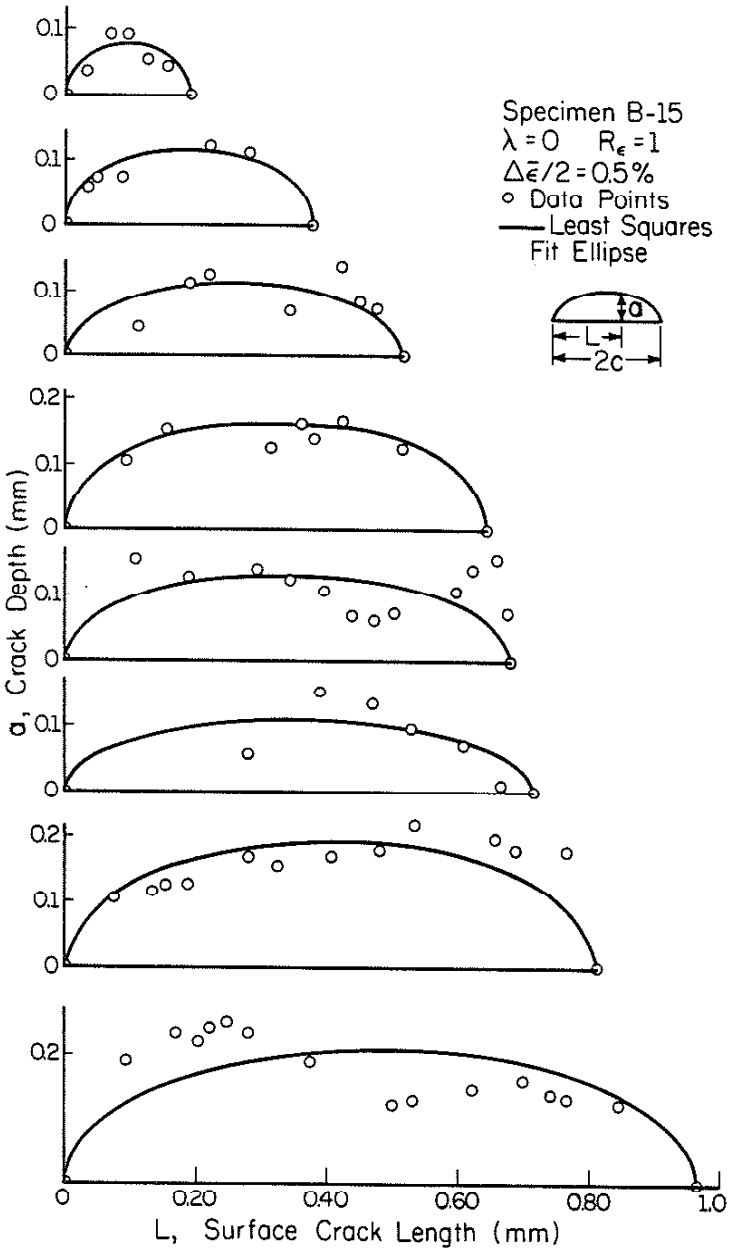

Figure 14 Least squares fit ellipse crack profiles, $\lambda = 0$, $\Delta\bar{\varepsilon}/2 = 0.5$ percent, $R_\varepsilon = 0$

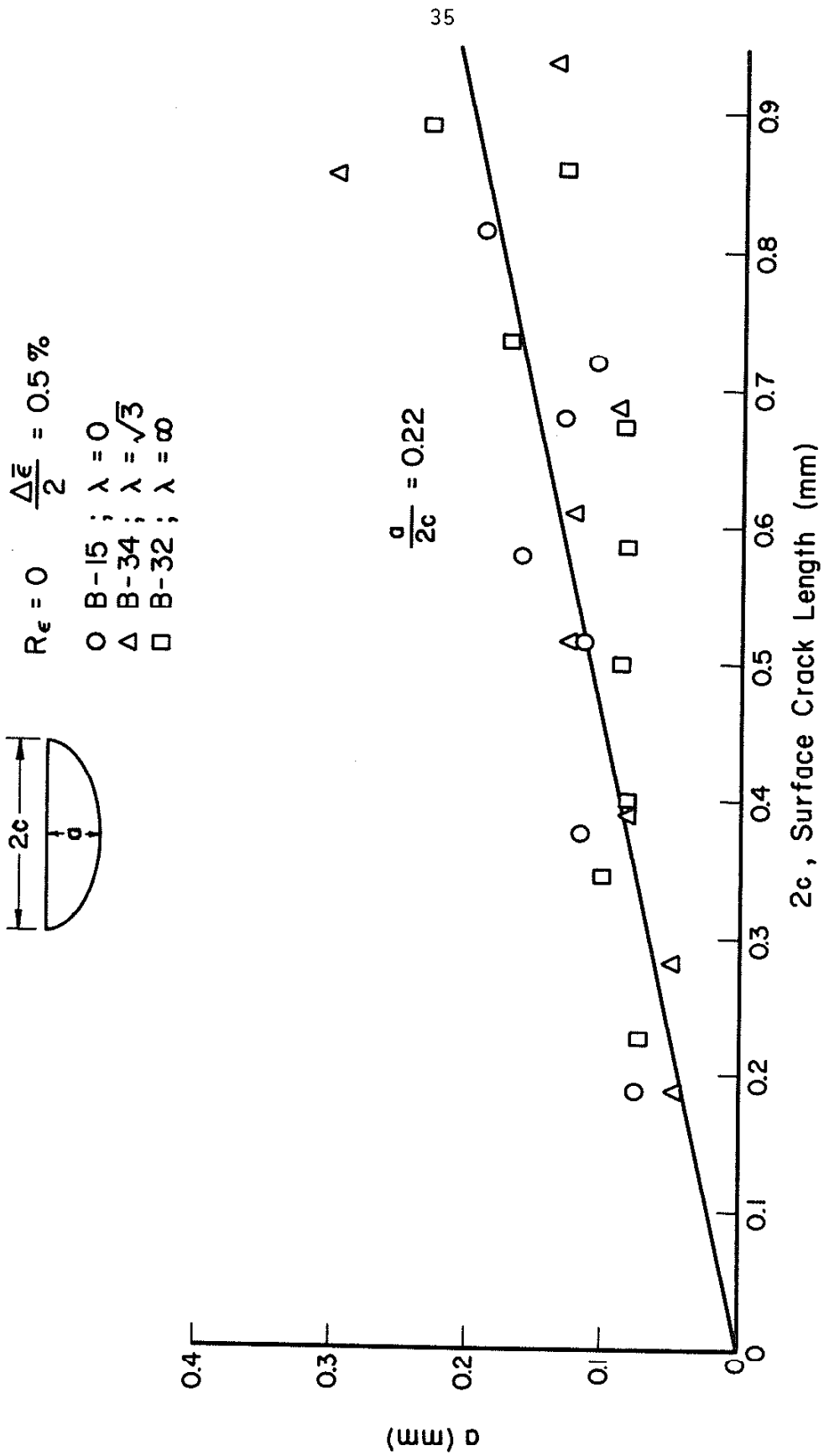

Figure 15 a versus 2c, = 0, , and $\bar{3}$, R = 0, /2 = 0.5 percent

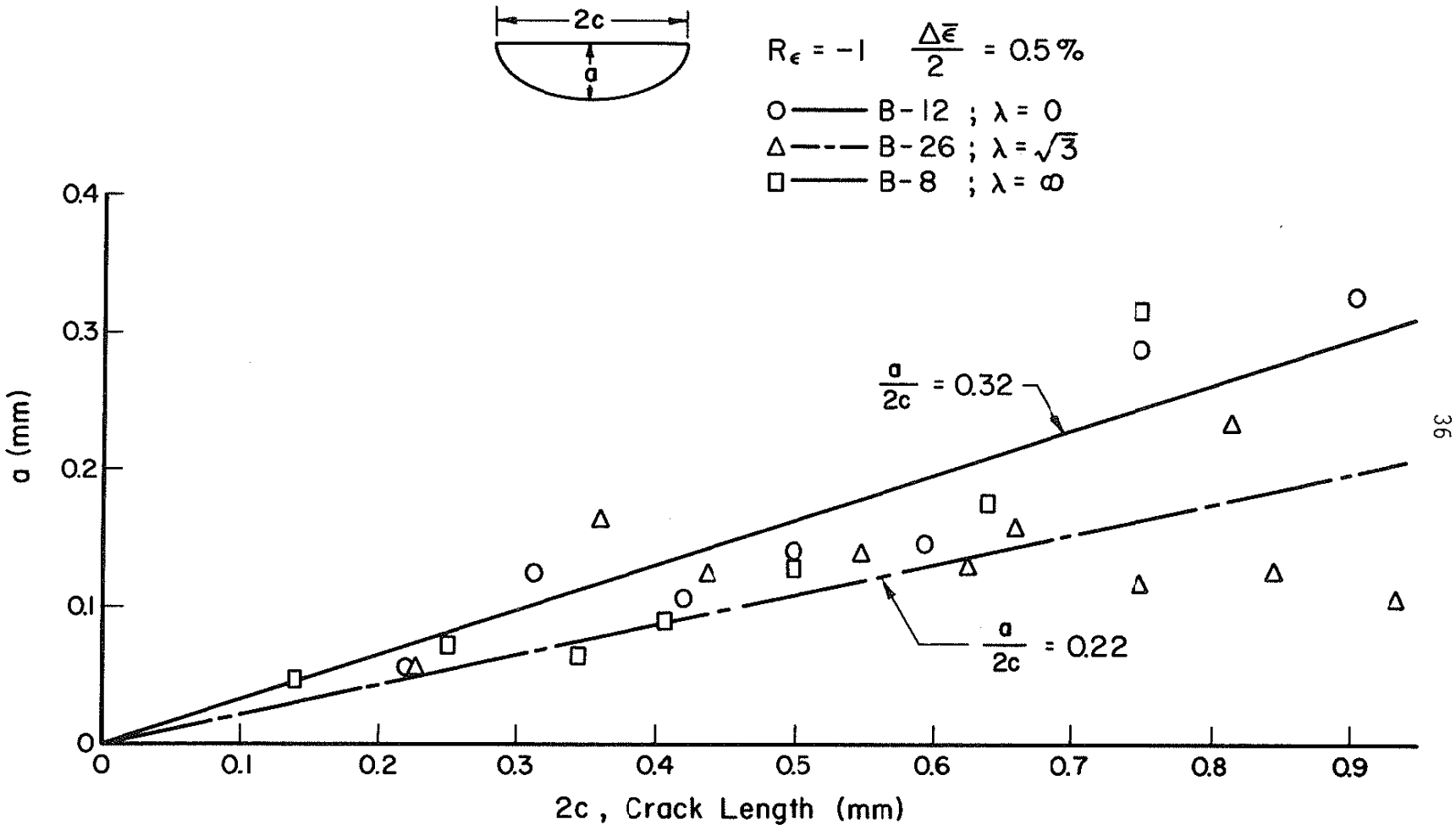

Figure 16 a versus 2c, = 0, and $\overline{3}$, R = -1, $\bar{}$/2 = 0.5 percent

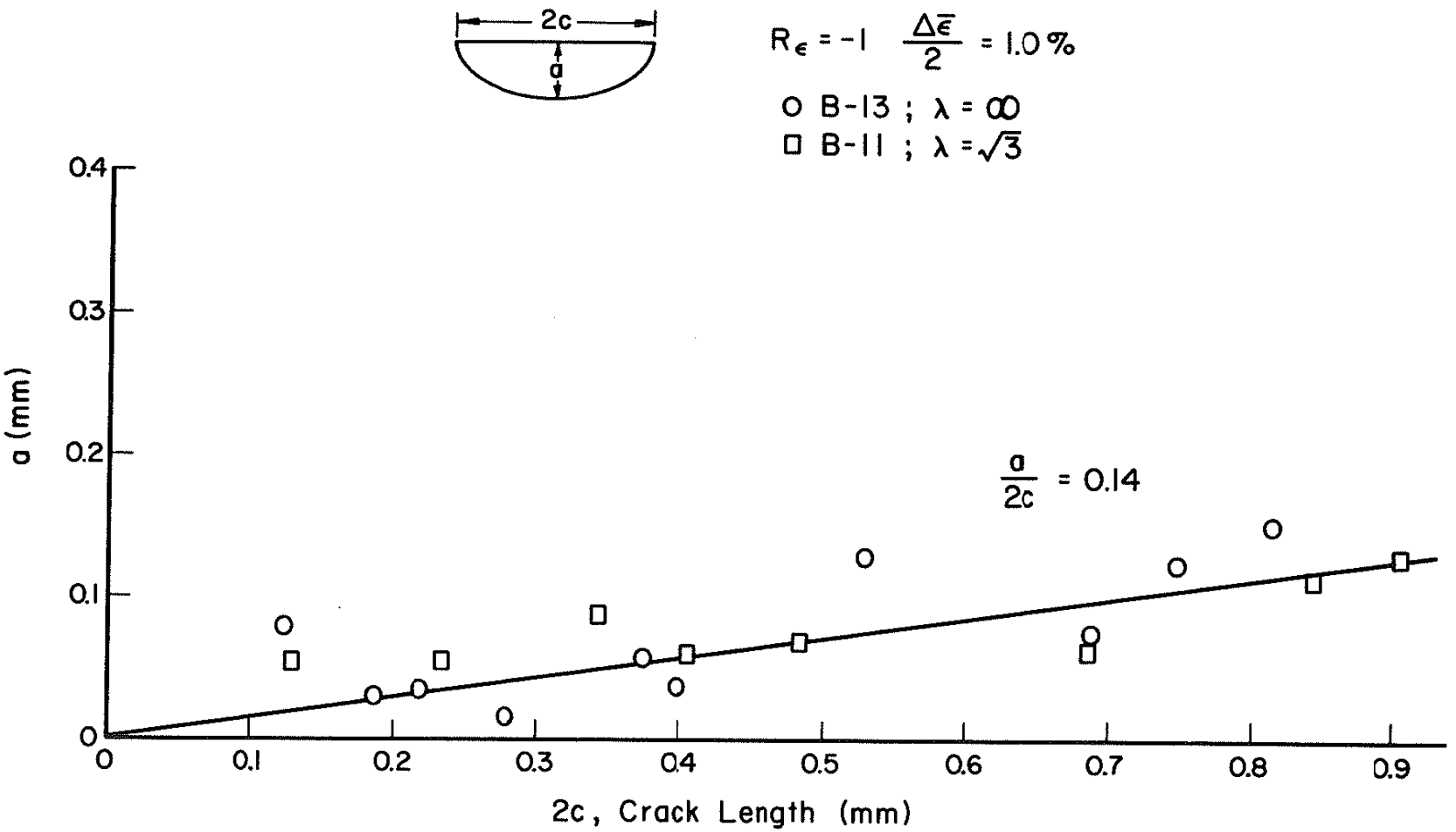

Figure 17 a versus 2c, = and $\overline{3}$, R = -1, $\bar{}$/2 = 1.0 percent

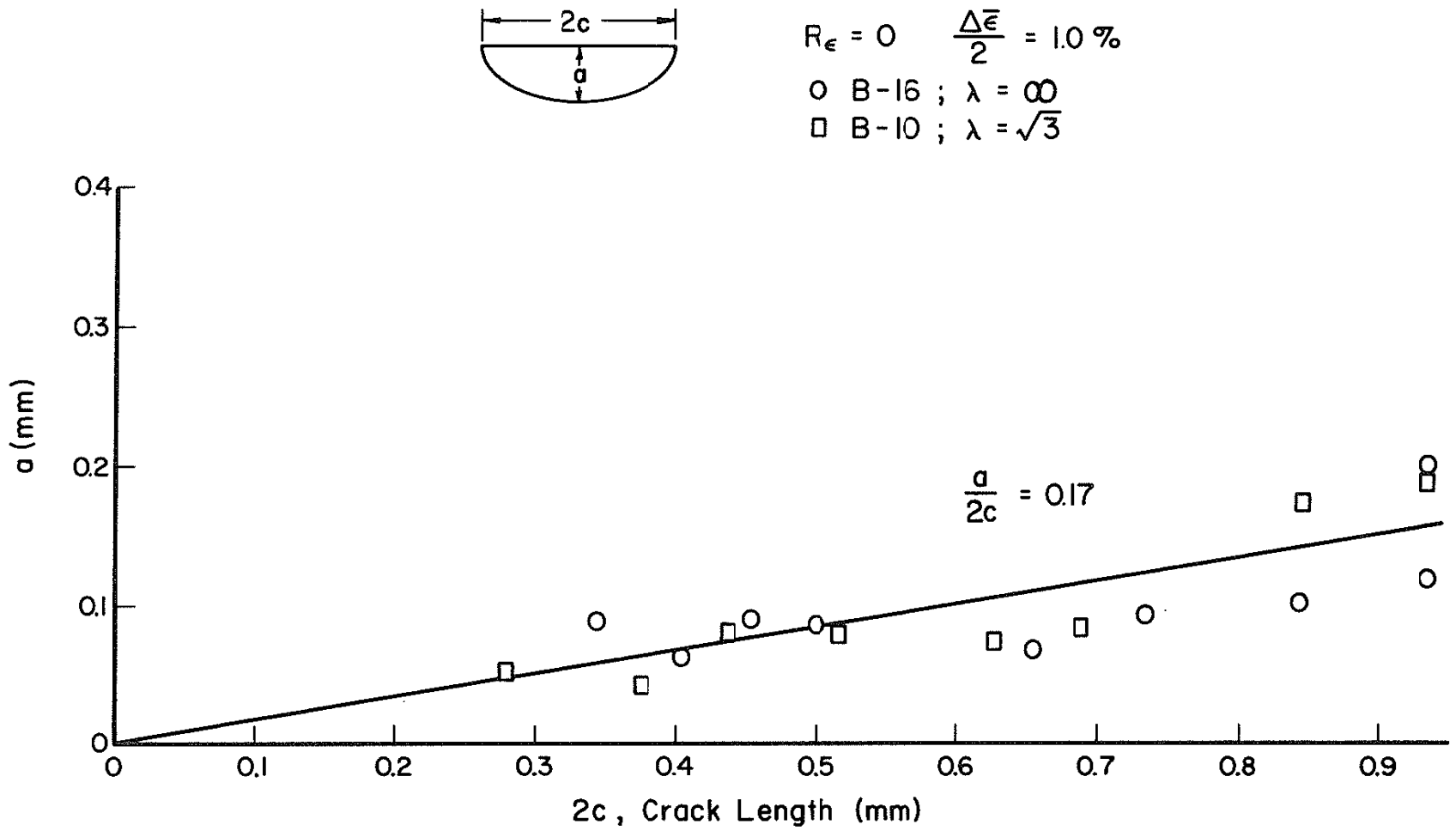

Figure 18 a versus 2c, = and $\sqrt{3}$, R = 0, $\bar{}$/2 = 1.0 percent

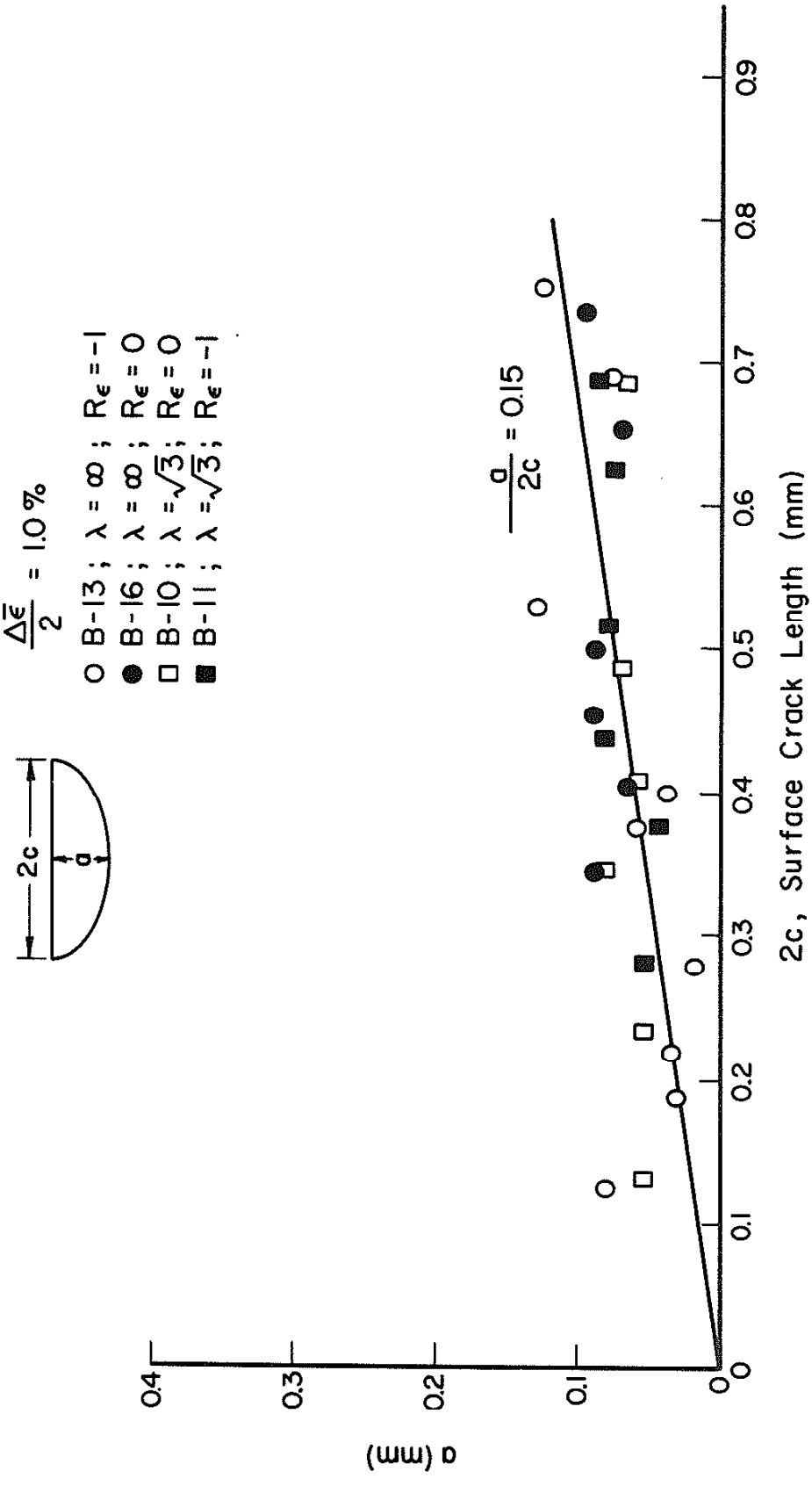

Figure 19 a versus 2c, = and $\bar{3}$, R = -1 and 0, /2 = 1.0 percent

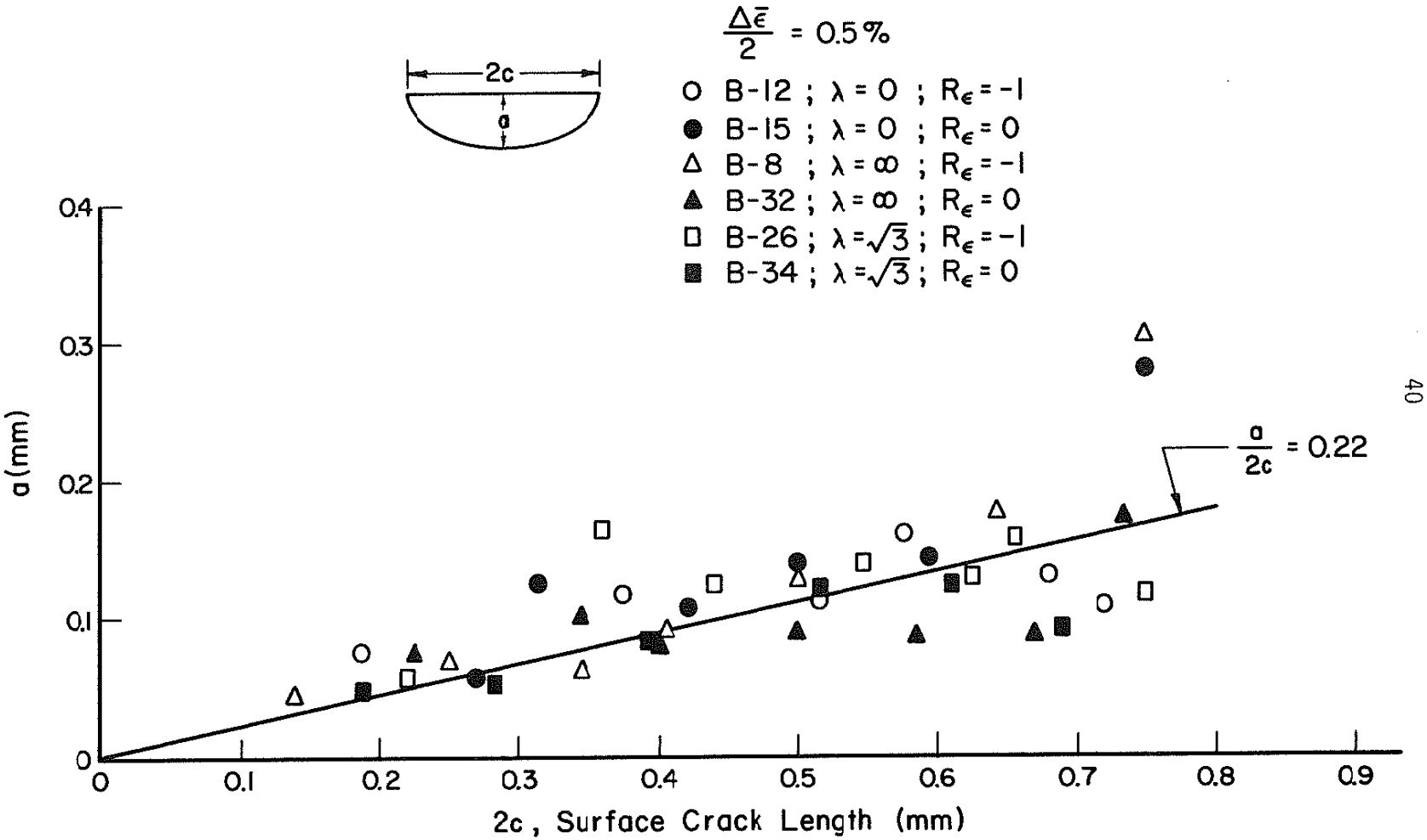

Figure 20 a versus 2c, = 0, and $\sqrt{3}$, R = -1 and 0, $\bar{\epsilon}$/2 = 0.5 percent

Figure 21 Combined loading crack at surface obstruction

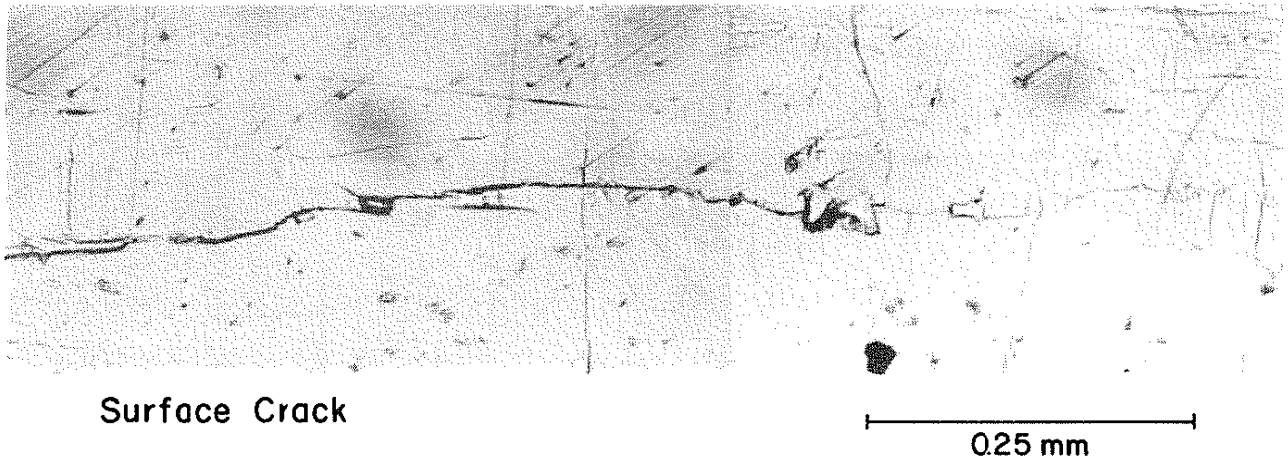

Figure 22 Torsion crack profile, $\Delta\bar{\epsilon}/2$ = 0.5 percent, R_ε = -1

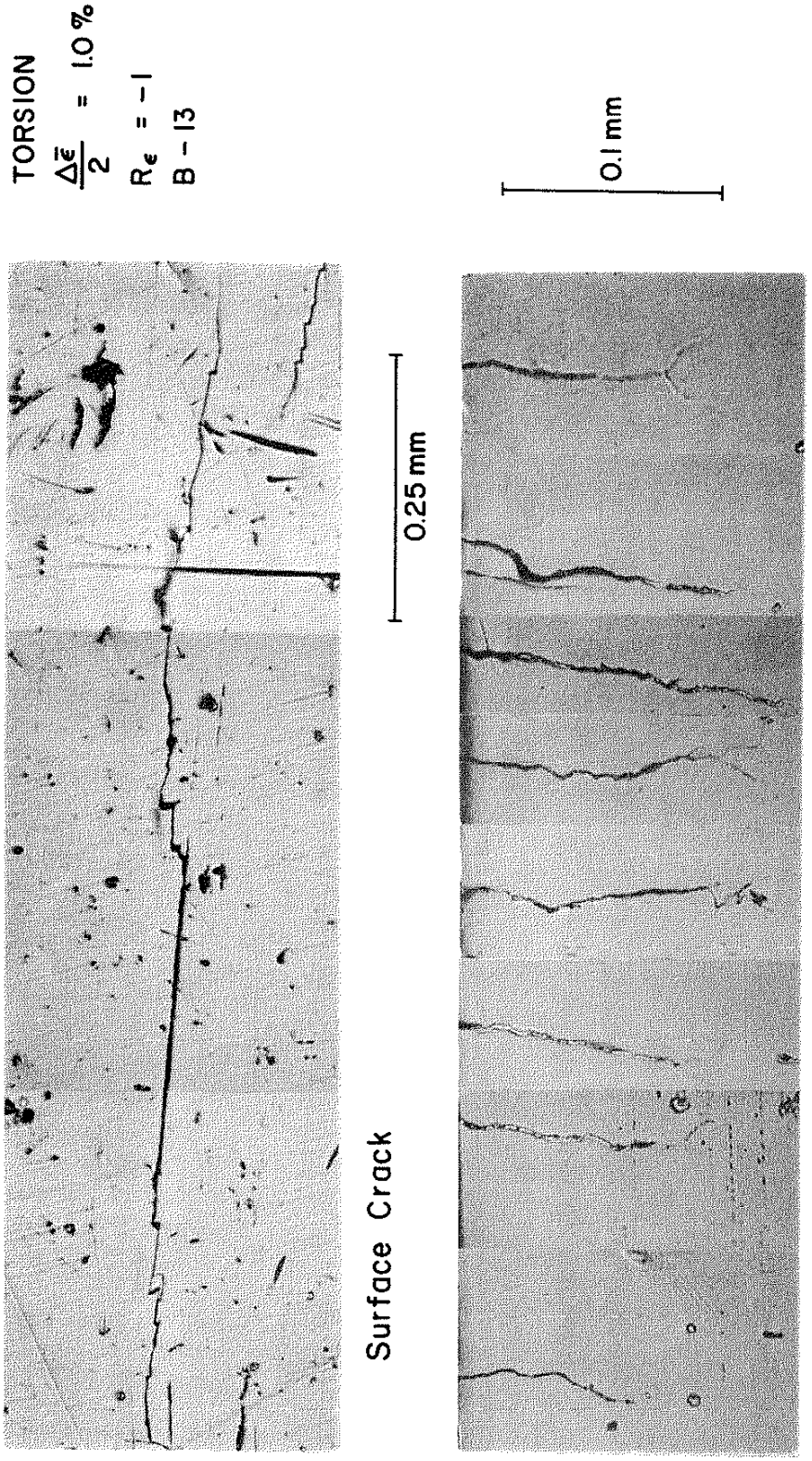

Figure 23 Torsion Crack Profile, $\Delta\bar{\varepsilon}/2$ = 1.0 Percent, R_ε = -1

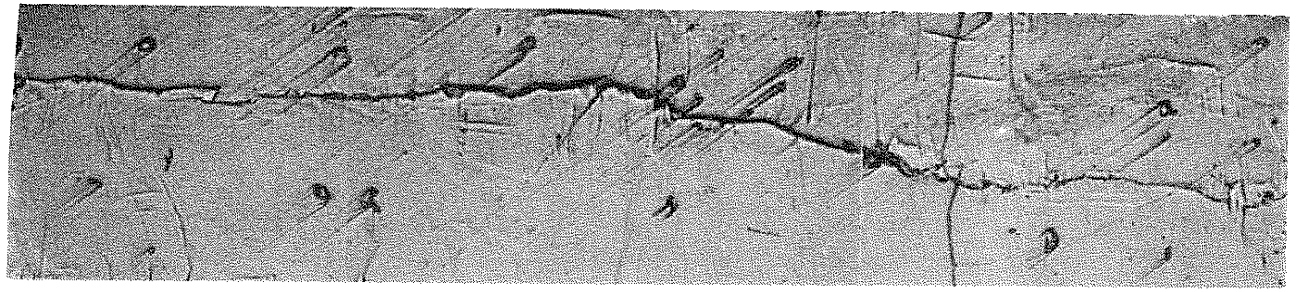

TORSION

$\frac{\Delta\bar{\epsilon}}{2}$ = 0.5 %

R_ϵ = 0

B - 32

Surface Crack

0.25 mm

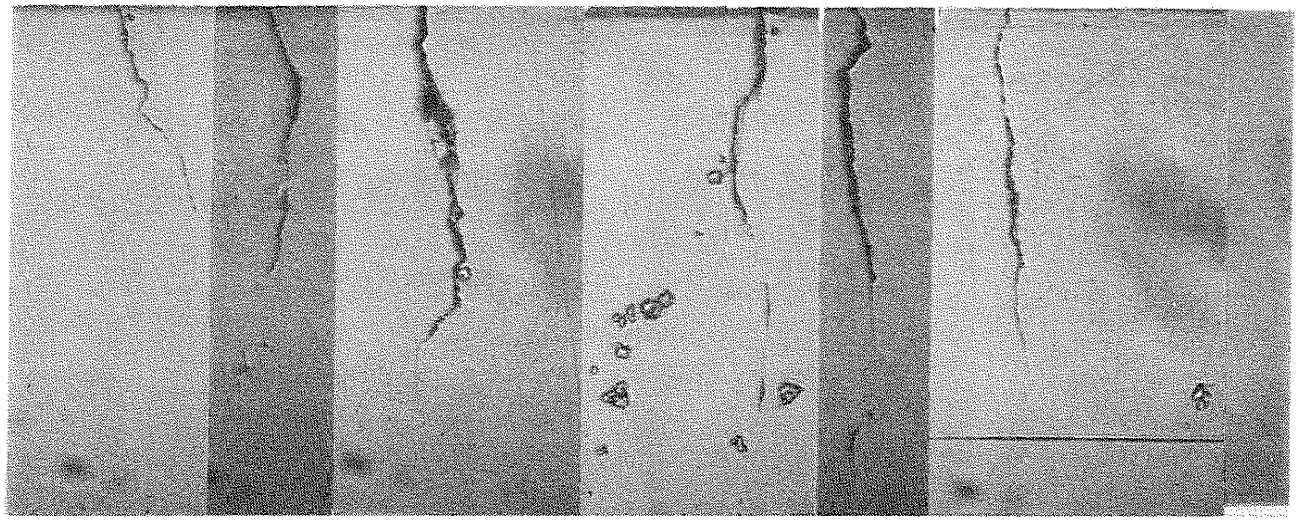

0.15 mm

Crack Depth

Figure 24 Torsion crack profile, $\Delta\bar{\epsilon}/2$ = 0.5 percent, R_ε = 0

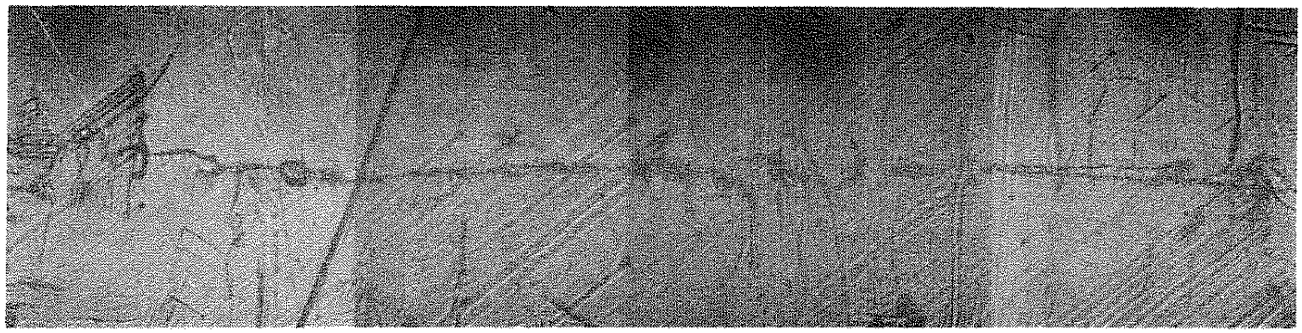

TORSION

$\frac{\Delta\bar{\epsilon}}{2}$ = 1.0 %

R_ϵ = 0

B – 16

Surface Crack

0.25 mm

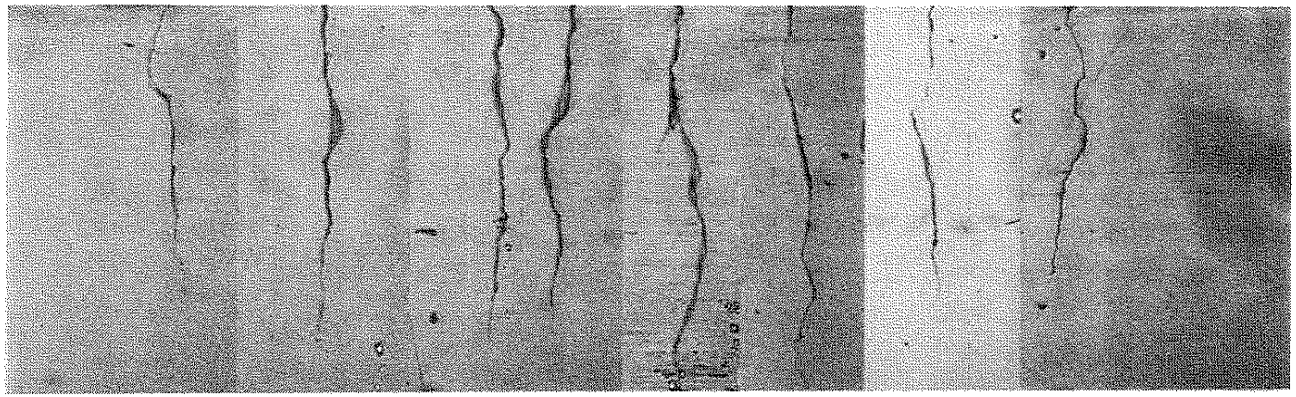

0.15 mm

Crack Depth

Figure 25 Torsion crack profile, $\Delta\bar{\epsilon}/2$ = 1.0 percent, R_ϵ = 0

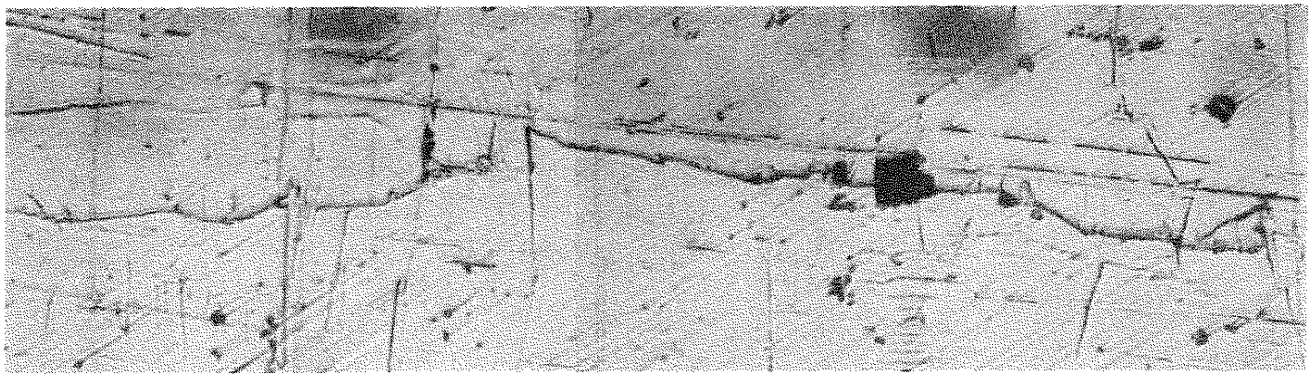

COMBINED
TENSION - TORSION

$\frac{\Delta\bar{\epsilon}}{2}$ = 0.5 %

R_ϵ = -1

B - 26

Surface Crack

0.25 mm

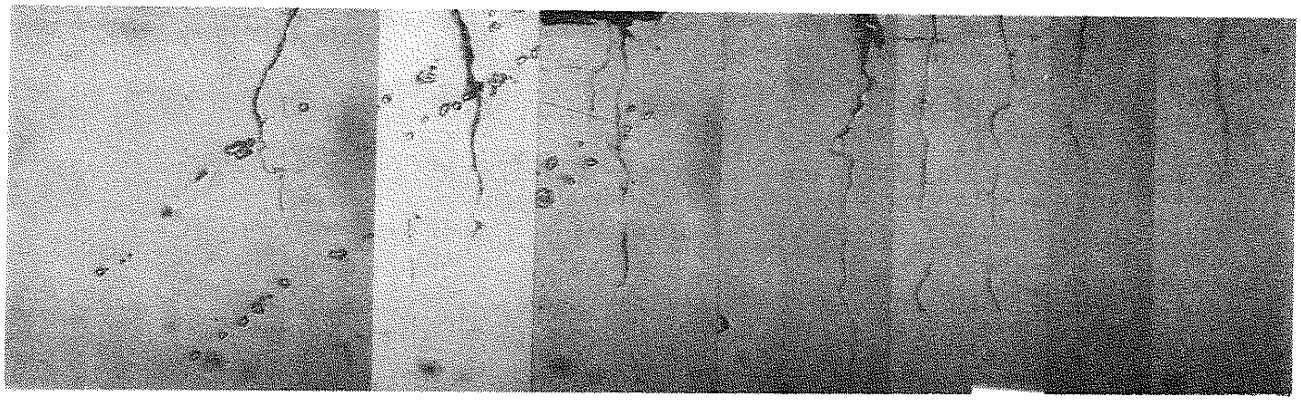

0.15 mm

Crack Depth

Figure 26 Combined tension-torsion crack profile, $\Delta\bar{\epsilon}/2$ = 0.5 percent, R_ϵ = -1

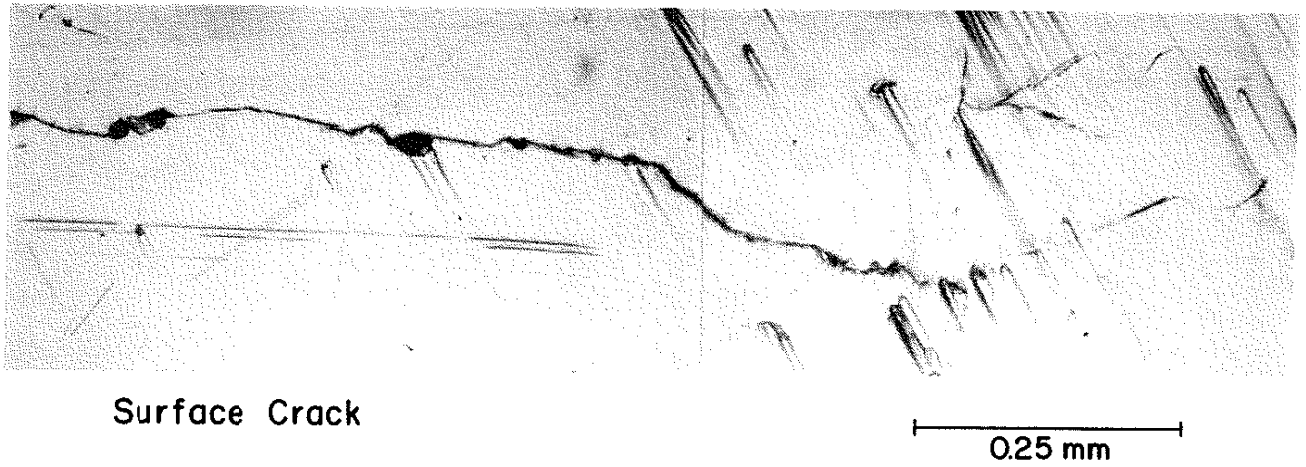

Figure 27 Combined tension-torsion crack profile, $\Delta\bar{\epsilon}/2$ = 0.5 percent, R_ε = 0

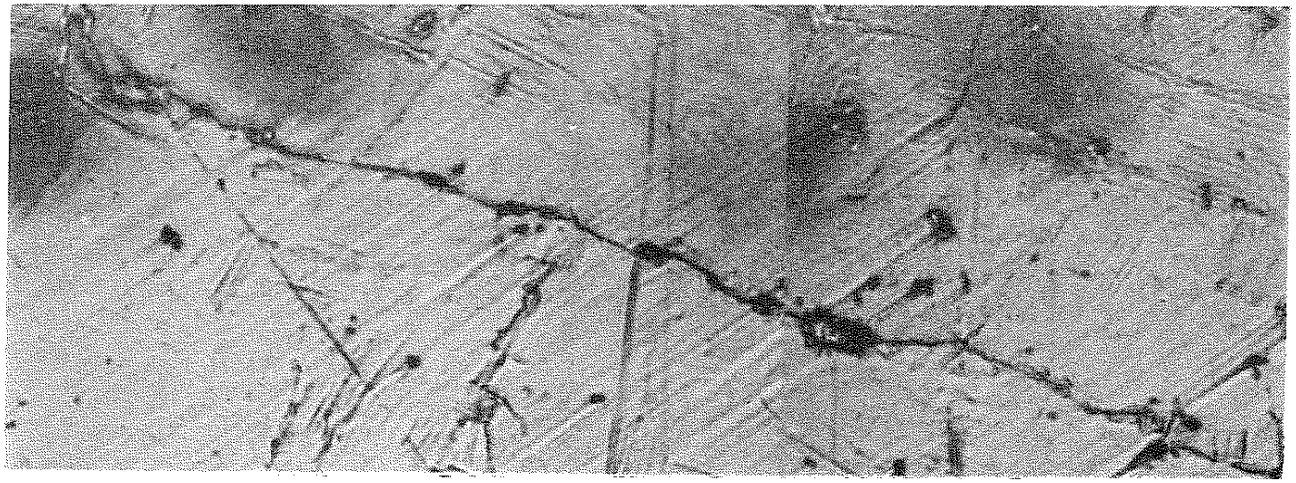

COMBINED
TENSION-TORSION

$\frac{\Delta\bar{\epsilon}}{2}$ = 1.0 %

R_ϵ = 0

B - 10

Surface Crack

0.25 mm

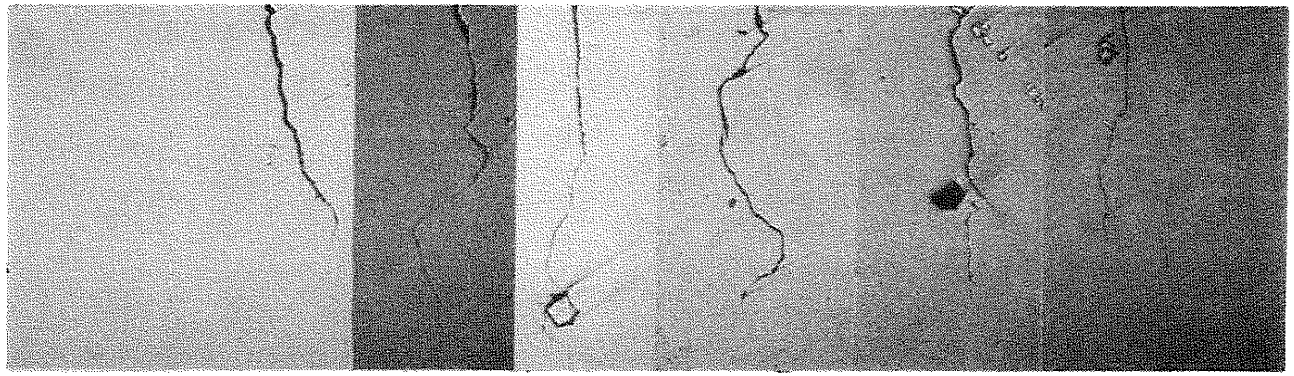

0.15 mm

Crack Depth

Figure 28 Combined tension-torsion crack profile, $\Delta\bar{\epsilon}/2$ = 1.0 percent, R_ϵ = 0

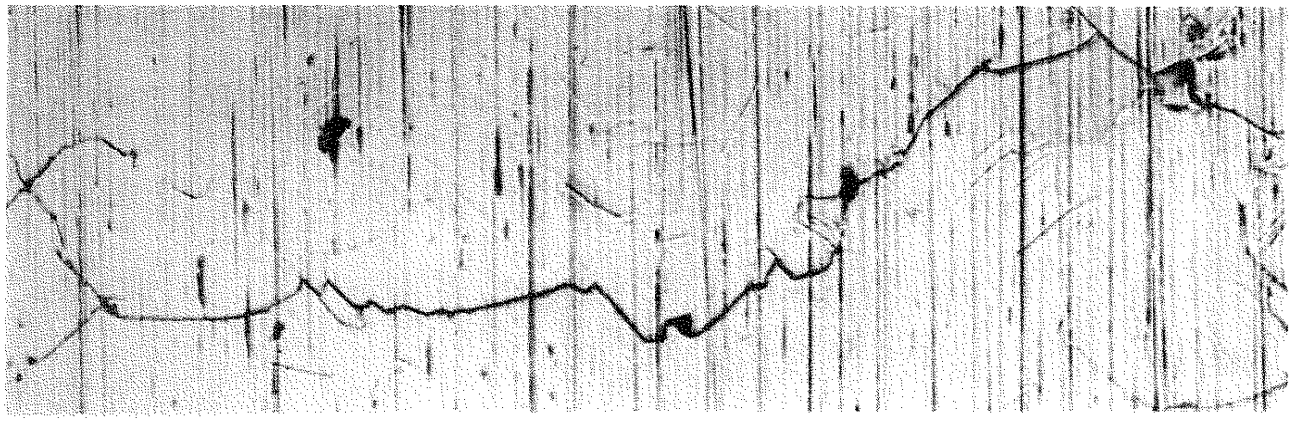

TENSION

$\frac{\Delta\bar{\epsilon}}{2}$ = 0.5 %

R_ϵ = -1

B-12

Surface Crack

0.25 mm

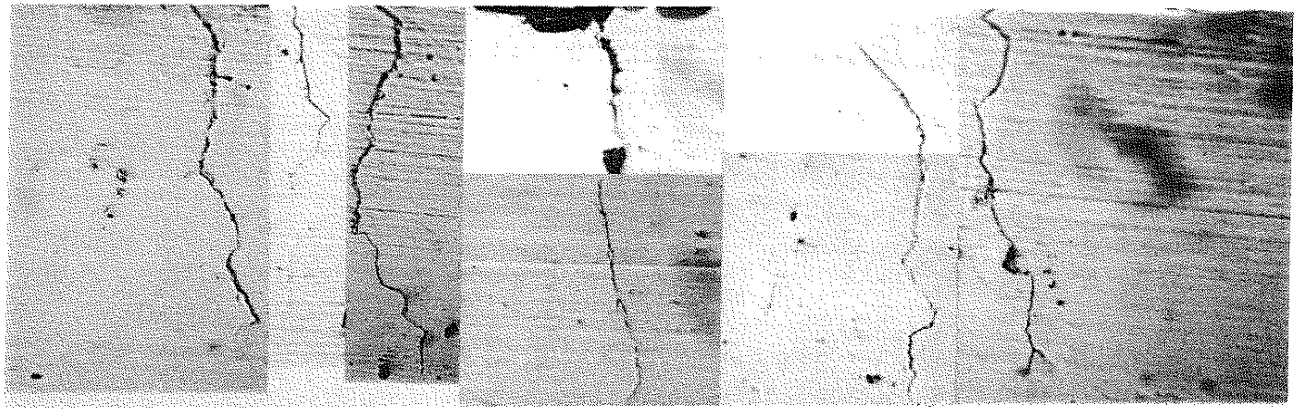

0.2 mm

Crack Depth

Figure 29 Tension crack profile, $\Delta\bar{\epsilon}/2$ = 0.5 percent, R_ϵ = -1

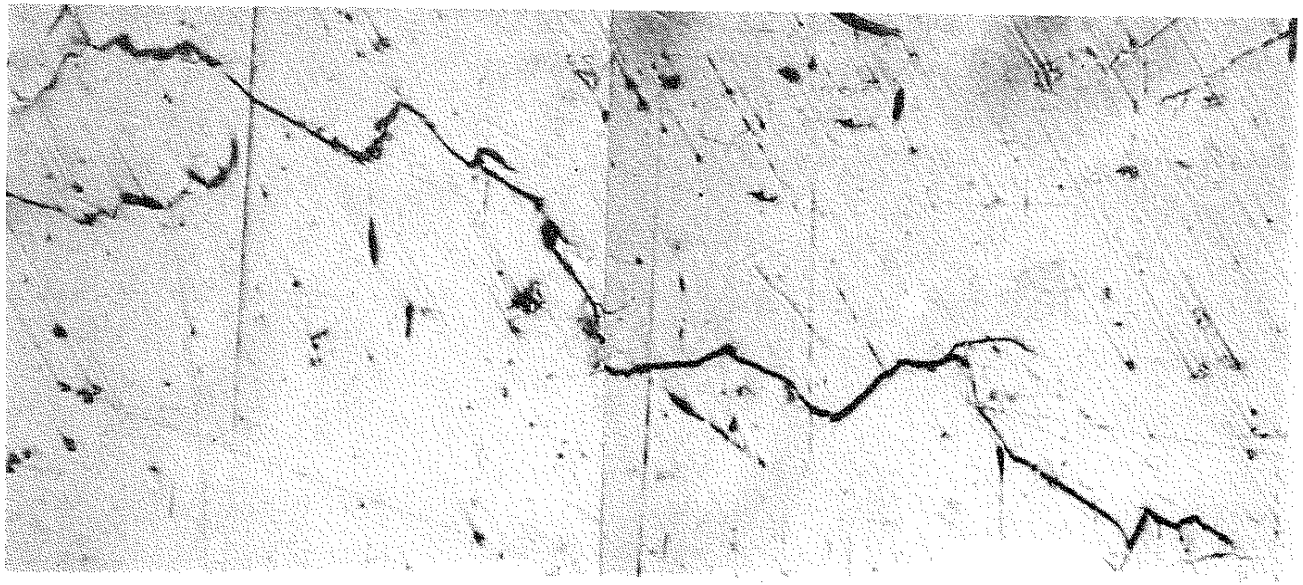

TENSION

$\frac{\Delta\bar{\epsilon}}{2}$ = 0.5 %

R_ϵ = 0

B-15

Surface Crack

0.25 mm

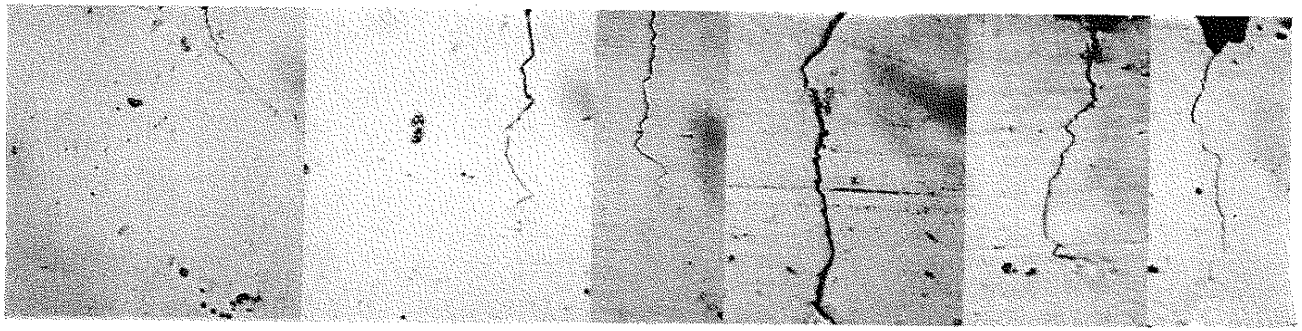

0.15 mm

Crack Depth

Figure 30 Tension crack profile, $\Delta\bar{\epsilon}/2$ = 0.5 percent, R_ϵ = 0

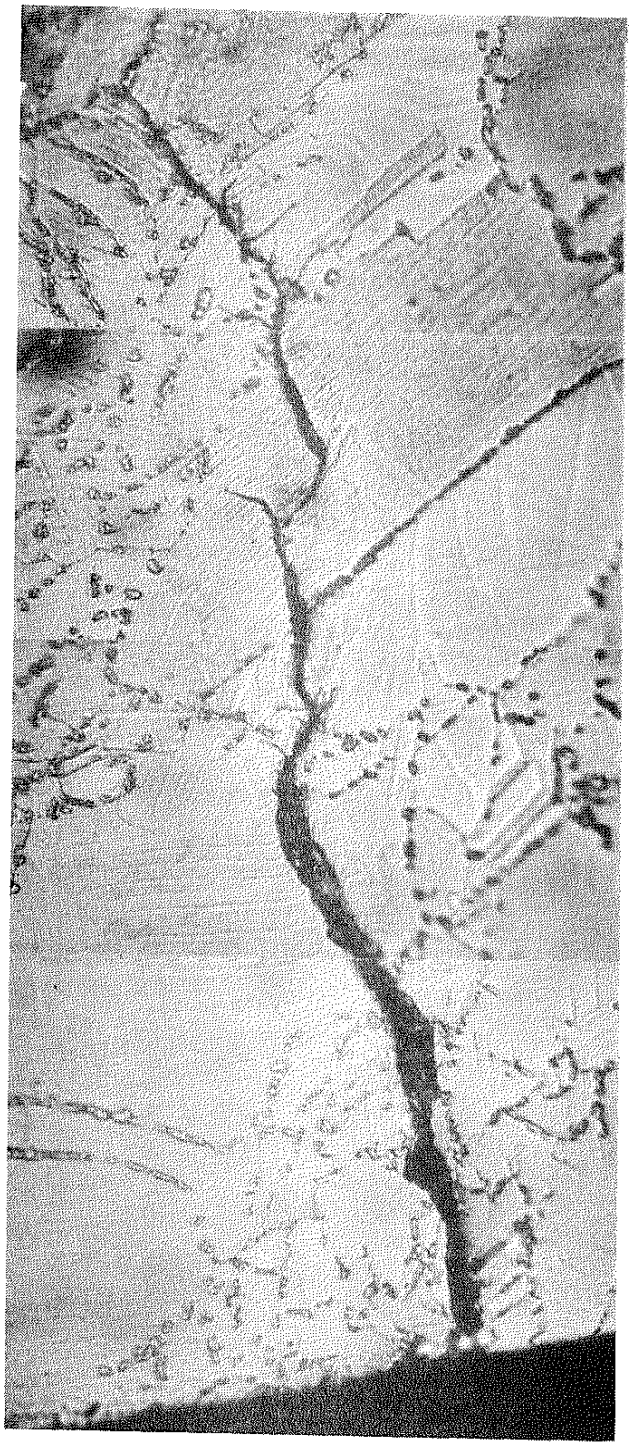

Figure 31 Etched torsional specimen

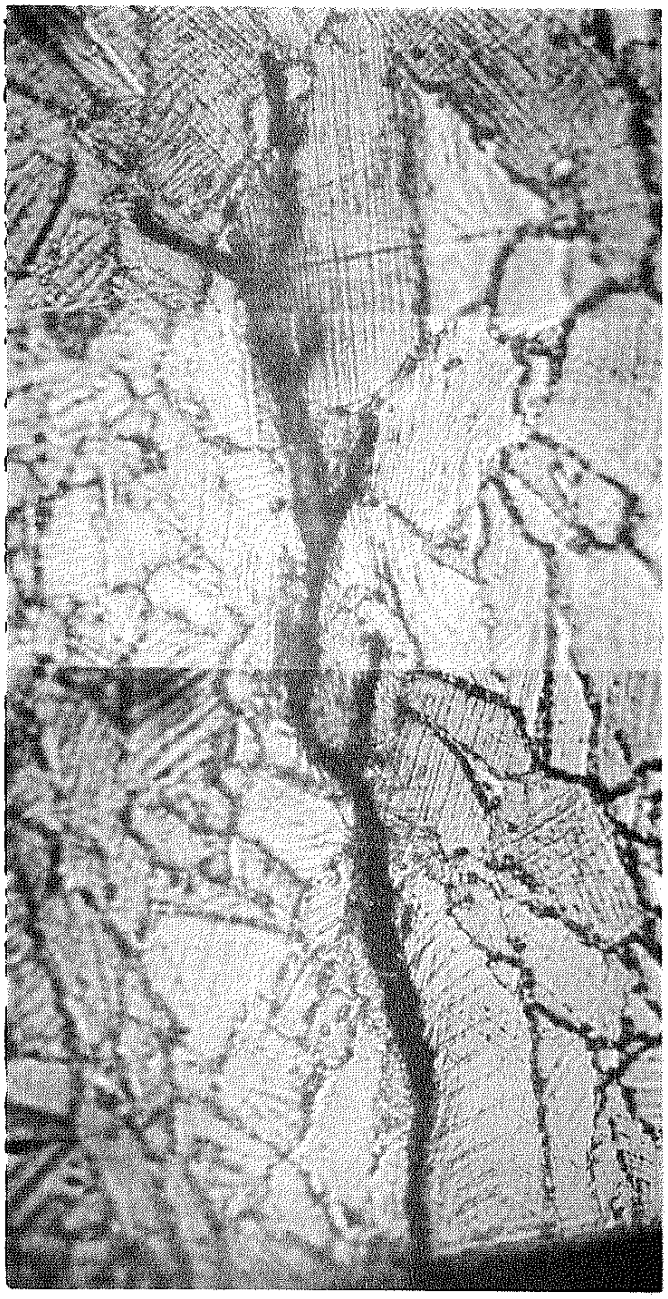

Figure 32 Etched torsional specimen

Figure 33 Intersection of torsion crack with grain boundary

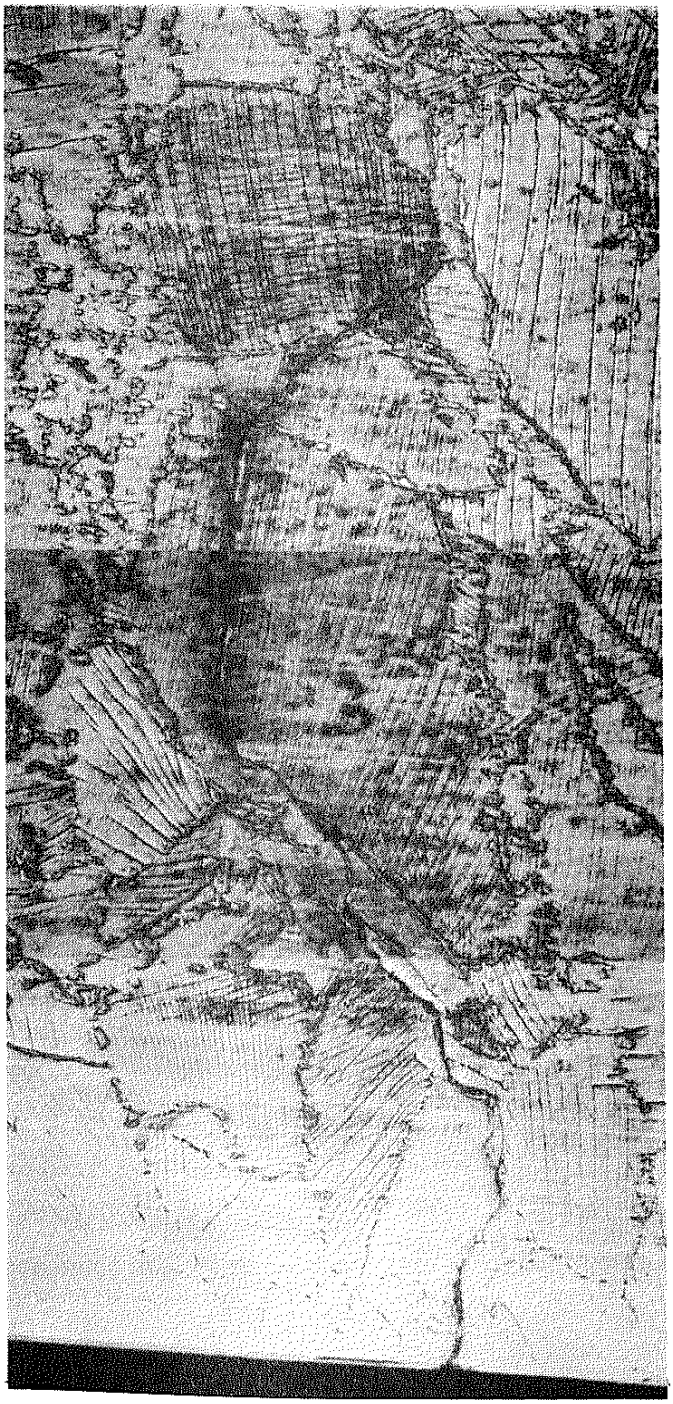

Figure 34 Etched combined tension-torsion specimen

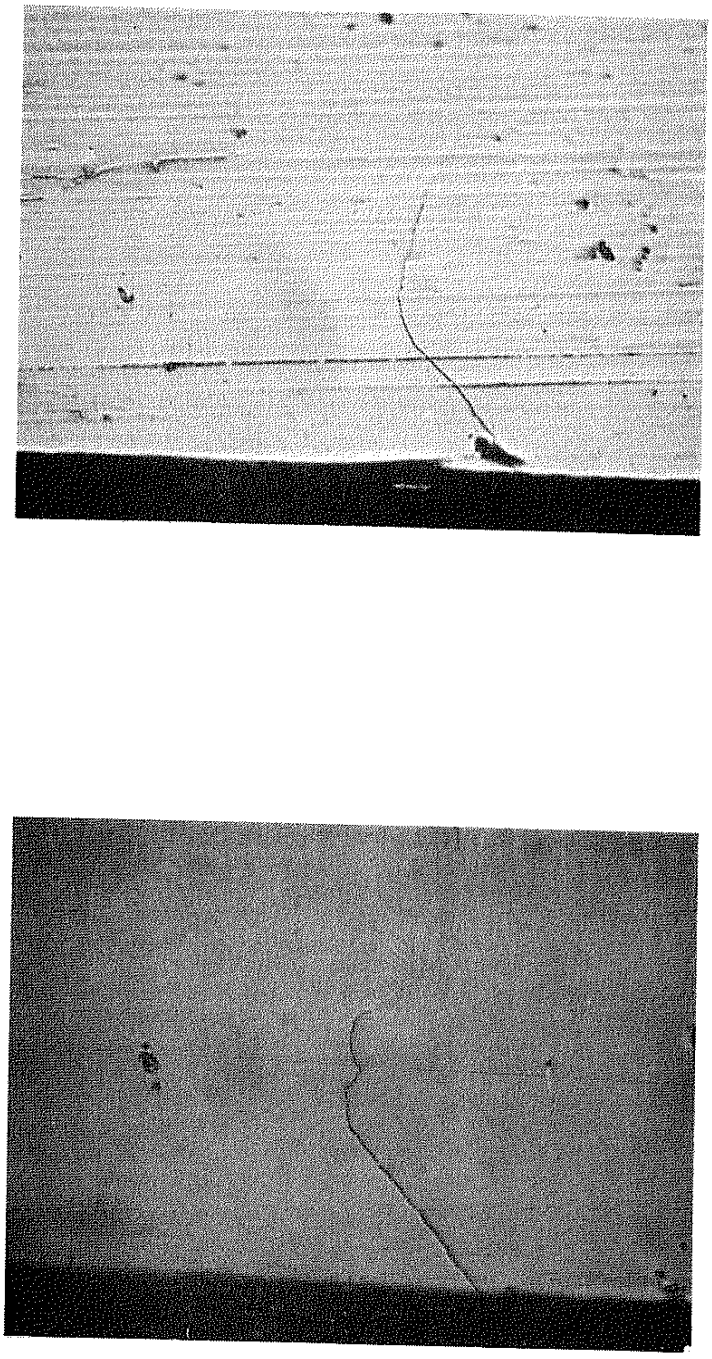

Figure 35 Cracks showing Stage I to Stage II transition

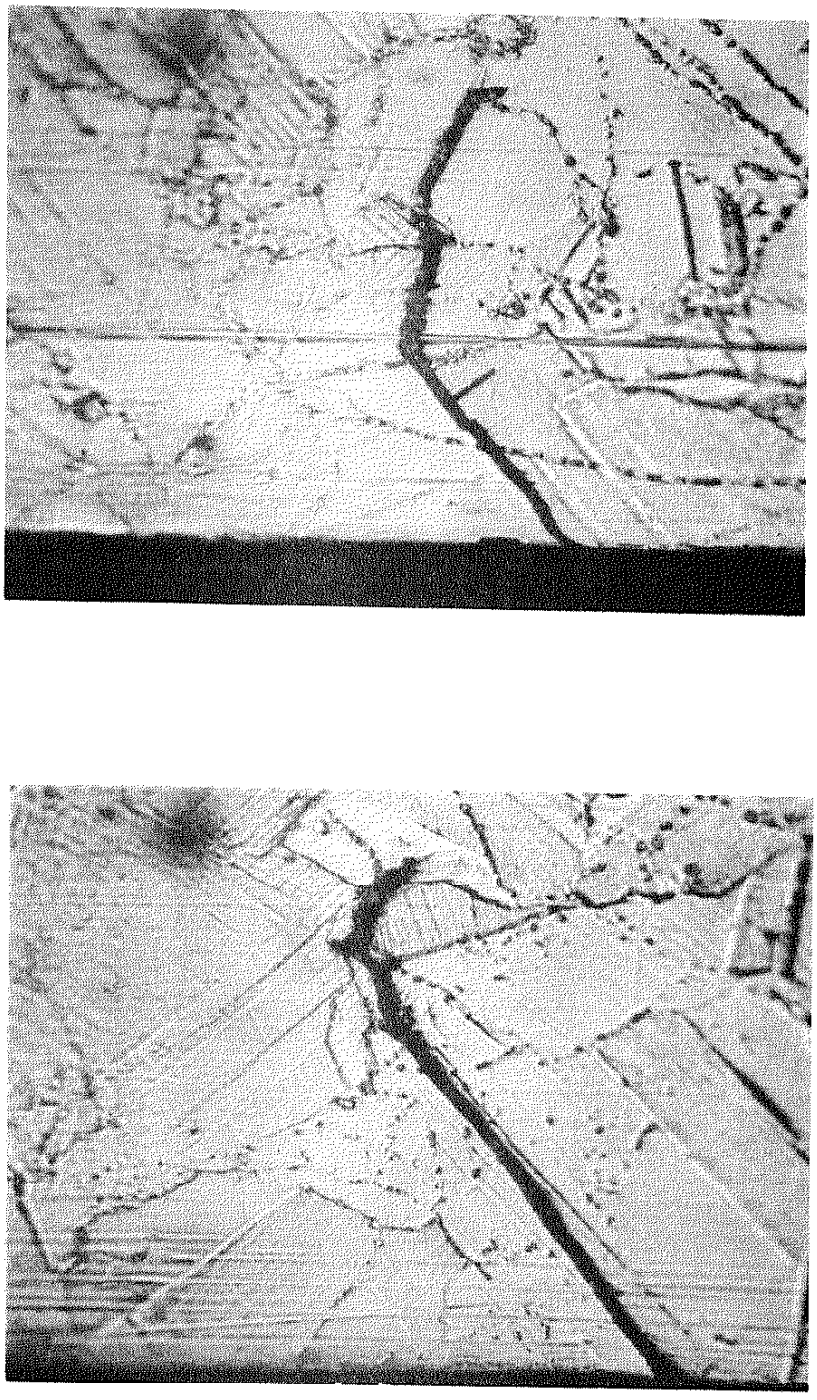

Figure 36 Etching of specimen showing Stage I to Stage II transition

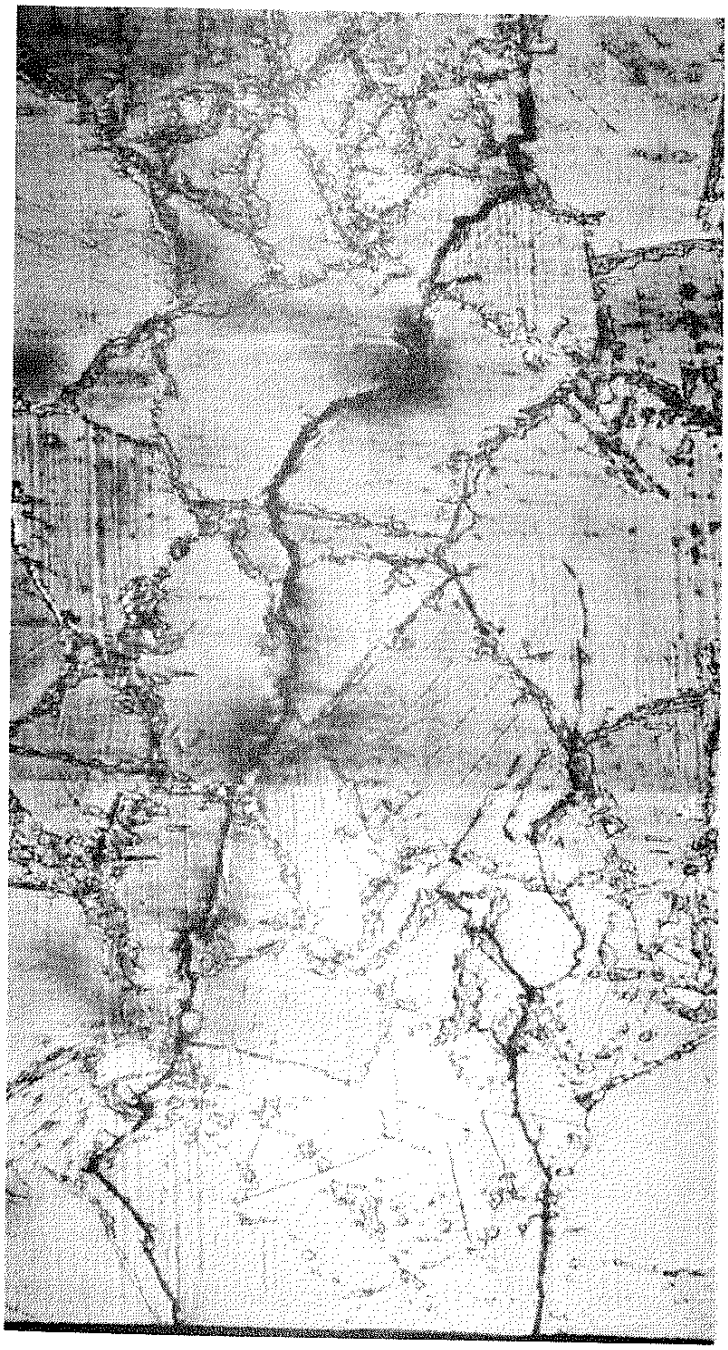

Figure 37 Etched tensile specimen

APPENDIX

On the following pages are shown various stages of crack growth for each of the ten specimens from which data was collected. All dimensions are in millimeters.

Table A.1 Results of Crack Sectioning

SPECIMEN B - 8

$R_\varepsilon = -1$

$\Delta/2 = 0.5\%$

2c = 0.14		2c = 0.25		2c = 0.34	
L	a	L	a	L	a
0.14	0.00	0.25	0.00	0.34	0.00
0.13	0.04	0.23	0.07	0.33	0.04
0.11	0.05	0.22	0.07	0.31	0.04
0.09	0.04	0.20	0.07	0.24	0.04
0.05	0.03	0.19	0.06	0.16	0.06
		0.14	0.08	0.13	0.06
		0.13	0.06	0.09	0.07
		0.11	0.08		
		0.08	0.05		
		0.06	0.05		
		0.03	0.05		

2c = 0.41		2c = 0.50		2c = 0.64		2c = 0.75		2c = 0.97	
L	a	L	a	L	a	L	a	L	a
0.41	0.00	0.50	0.00	0.64	0.00	0.75	0.00	0.97	0.00
0.39	0.02	0.44	0.04	0.63	0.09	0.69	0.20	0.93	0.03
0.37	0.04	0.41	0.11	0.58	0.10	0.66	0.29	0.87	0.13
0.36	0.04	0.38	0.09	0.52	0.11	0.59	0.34	0.80	0.20
0.34	0.04	0.30	0.16	0.48	0.16	0.56	0.31	0.72	0.30
0.33	0.04	0.27	0.16	0.41	0.19	0.50	0.31	0.59	0.31
0.27	0.07	0.22	0.13	0.36	0.18	0.45	0.30	0.52	0.36
0.23	0.09	0.17	0.09	0.31	0.19	0.19	0.22	0.44	0.34
0.22	0.09	0.09	0.11	0.27	0.20	0.14	0.19	0.34	0.34
0.19	0.09			0.23	0.17	0.09	0.08	0.27	0.32
0.17	0.11			0.17	0.16			0.20	0.31
0.14	0.11			0.13	0.09				
0.13	0.12								
0.07	0.04								

Table A.2 Results of Crack Sectioning

SPECIMEN B - 13

$R_\varepsilon = -1$

$\Delta/2 = 1.0\%$

2c = 0.13		2a = 0.19		2c = 0.22		2c = 0.28		2c = 0.38	
L	a	L	a	L	a	L	a	L	a
0.13	0.00	0.19	0.00	0.22	0.00	0.28	0.00	0.38	0.00
0.06	0.08	0.17	0.03	0.19	0.03	0.23	0.01	0.36	0.05
0.02	0.05	0.11	0.03	0.14	0.03	0.17	0.01	0.30	0.05
		0.06	0.03	0.08	0.04	0.16	0.03	0.27	0.05
		0.03	0.02	0.07	0.03	0.13	0.02	0.25	0.07
						0.10	0.02	0.23	0.06
								0.19	0.05
								0.14	0.05
								0.05	0.02

2c = 0.40		2c = 0.53		2c = 0.69		2c = 0.75		2c = 0.81	
L	a	L	a	L	a	L	a	L	a
0.40	0.00	0.53	0.00	0.69	0.00	0.75	0.00	0.81	0.00
0.33	0.06	0.49	0.02	0.66	0.08	0.70	0.06	0.78	0.06
0.20	0.04	0.47	0.08	0.62	0.09	0.63	0.09	0.72	0.17
0.13	0.03	0.45	0.09	0.58	0.08	0.59	0.11	0.53	0.16
0.07	0.02	0.42	0.09	0.52	0.09	0.59	0.16	0.43	0.14
0.06	0.01	0.38	0.10	0.44	0.07	0.52	0.11	0.31	0.17
		0.28	0.12	0.42	0.08	0.44	0.10	0.25	0.13
		0.14	0.12	0.39	0.10	0.33	0.09	0.17	0.11
		0.08	0.12	0.34	0.04	0.31	0.10	0.11	0.06
		0.07	0.11	0.23	0.04	0.28	0.09	0.05	0.02
		0.04	0.10	0.16	0.03	0.22	0.10		
				0.11	0.03	0.20	0.11		
						0.14	0.12		
						0.08	0.11		

Table A.3 Results of Crack Sectioning

SPECIMEN B - 32

$R_\varepsilon = 0$

$\Delta/2 = 0.5\%$

2c = 0.23		2c = 0.34		2c = 0.40		2c = 0.50		2c = 0.59	
L	a	L	a	L	a	L	a	L	a
0.23	0.00	0.34	0.00	0.40	0.00	0.50	0.00	0.59	0.00
0.22	0.06	0.33	0.06	0.34	0.07	0.46	0.06	0.54	0.03
0.19	0.07	0.31	0.07	0.30	0.04	0.41	0.08	0.51	0.06
0.14	0.06	0.26	0.09	0.23	0.09	0.36	0.09	0.46	0.04
0.11	0.07	0.23	0.10	0.20	0.09	0.29	0.11	0.36	0.09
0.05	0.06	0.17	0.09	0.11	0.07	0.23	0.09	0.27	0.08
		0.15	0.09	0.06	0.09	0.12	0.04	0.19	0.05
		0.09	0.09			0.04	0.02	0.14	0.12
		0.03	0.07					0.05	0.09

2c = 0.67		2c = 0.73		2c = 0.86		2c = 1.0		2c = 0.89	
L	a	L	a	L	a	L	a	L	a
0.67	0.00	0.73	0.00	0.86	0.00	1.0	0.00	0.89	0.00
0.61	0.08	0.63	0.09	0.77	0.06	0.88	0.14	0.72	0.16
0.55	0.07	0.53	0.17	0.69	0.09	0.80	0.24	0.59	0.23
0.50	0.06	0.44	0.20	0.56	0.16	0.75	0.24	0.53	0.23
0.47	0.06	0.38	0.20	0.47	0.16	0.66	0.27	0.43	0.21
0.41	0.07	0.30	0.16	0.42	0.16	0.59	0.27	0.28	0.17
0.33	0.08	0.21	0.15	0.34	0.13	0.53	0.29	0.16	0.16
0.27	0.13	0.16	0.12	0.26	0.08	0.48	0.26	0.06	0.11
0.20	0.08	0.09	0.11	0.17	0.09	0.41	0.19		
0.16	0.08	0.03	0.07	0.09	0.07	0.31	0.23		
0.11	0.05					0.27	0.11		
						0.19	0.09		
						0.16	0.09		
						0.06	0.07		

Table A.4 Results of Crack Sectioning

SPECIMEN B - 16

$R_\epsilon = 0$

$\Delta/2 = 1.0\%$

2c = 0.34		2c = 0.41		2c = 0.45		2c = 0.50		2c = 0.66	
L	a	L	a	L	a	L	a	L	a
0.34	0.00	0.41	0.00	0.45	0.00	0.50	0.00	0.66	0.00
0.33	0.08	0.39	0.02	0.45	0.01	0.45	0.02	0.58	0.07
0.27	0.08	0.30	0.08	0.22	0.09	0.37	0.06	0.48	0.03
0.20	0.08	0.25	0.04	0.16	0.08	0.34	0.08	0.45	0.07
0.17	0.08	0.23	0.05	0.05	0.07	0.30	0.06	0.42	0.07
0.11	0.08	0.19	0.08			0.24	0.10	0.38	0.07
0.08	0.07					0.20	0.11	0.31	0.08
0.02	0.06					0.17	0.11	0.27	0.08
						0.12	0.07	0.17	0.05
						0.06	0.05		

2c = 0.73		2c = 0.84		2c = 0.94		2c = 1.0	
L	a	L	a	L	a	L	a
0.73	0.00	0.84	0.00	0.94	0.00	1.0	0.0
0.71	0.02	0.81	0.03	0.83	0.08	0.84	0.14
0.66	0.07	0.73	0.08	0.81	0.08	0.73	0.06
0.59	0.08	0.72	0.09	0.69	0.08	0.63	0.20
0.53	0.09	0.66	0.08	0.64	0.09	0.53	0.20
0.48	0.09	0.61	0.08	0.55	0.10	0.45	0.20
0.44	0.09	0.57	0.08	0.50	0.11	0.38	0.17
0.31	0.08	0.53	0.09	0.44	0.11	0.25	0.17
		0.47	0.09	0.38	0.11	0.13	0.13
		0.41	0.10	0.28	0.12		
		0.31	0.11	0.15	0.08		
		0.20	0.10	0.06	0.08		
		0.14	0.10				

Table A.5 Results of Crack Sectioning

SPECIMEN B - 26

$R_\varepsilon = -1$

$\Delta/2 = 0.5\%$

2c = 0.22		2c = 0.36		2c = 0.44		2c = 0.55		2c = 0.63	
L	a	L	a	L	a	L	a	L	a
0.22	0.00	0.36	0.00	0.44	0.00	0.55	0.00	0.63	0.00
0.17	0.02	0.34	0.06	0.43	0.04	0.48	0.08	0.53	0.03
0.14	0.06	0.31	0.13	0.36	0.07	0.44	0.08	0.46	0.07
0.10	0.07	0.28	0.13	0.33	0.09	0.41	0.13	0.42	0.08
0.07	0.06	0.25	0.17	0.28	0.18	0.34	0.14	0.34	0.10
		0.16	0.16	0.22	0.18	0.33	0.11	0.31	0.15
		0.13	0.17	0.17	0.14	0.31	0.13	0.28	0.14
		0.11	0.16	0.11	0.08	0.25	0.15	0.17	0.15
		0.06	0.11	0.08	0.07	0.14	0.16	0.11	0.16
				0.08	0.04	0.09	0.14	0.06	0.16

2c = 0.66		2c = 0.75		2c = 0.81		2c = 0.84		2c = 0.94	
L	a	L	a	L	a	L	a	L	a
0.66	0.00	0.75	0.00	0.81	0.00	0.84	0.00	0.94	0.00
0.53	0.14	0.63	0.06	0.80	0.13	0.81	0.03	0.73	0.13
0.50	0.16	0.58	0.13	0.77	0.14	0.58	0.08	0.61	0.13
0.35	0.18	0.45	0.12	0.67	0.21	0.50	0.10	0.56	0.17
0.25	0.16	0.38	0.13	0.63	0.21	0.45	0.11	0.49	0.10
0.17	0.10	0.58	0.22	0.38	0.16	0.42	0.07		
0.11	0.08	0.25	0.10	0.56	0.23	0.30	0.16	0.34	0.05
		0.17	0.10	0.53	0.23	0.25	0.14	0.25	0.08
		0.10	0.09	0.28	0.16	0.20	0.11	0.17	0.05
		0.06	0.07	0.19	0.14	0.15	0.9	0.06	0.04
						0.11	0.06		

Table A.6 Results of Crack Sectioning

SPECIMEN B - 11

R_ε = -1

$\Delta/2$ = 1.0%

2c = 0.13		2c = 0.23		2c = 0.34		2c = 0.41	
L	a	L	a	L	a	L	a
0.13	0.00	0.23	0.00	0.34	0.00	0.41	0.00
0.09	0.05	0.19	0.04	0.25	0.07	0.38	0.03
0.08	0.05	0.12	0.05	0.23	0.09	0.26	0.06
0.06	0.06	0.09	0.07	0.19	0.11	0.20	0.04
0.02	0.05	0.06	0.04	0.11	0.06	0.13	0.05
		0.01	0.03	0.07	0.07	0.07	0.05
						0.04	0.07

2c = 0.48		2c = 0.69		2c = 0.84		2c = 0.91	
L	a	L	a	L	a	L	a
0.48	0.00	0.69	0.00	0.84	0.00	0.91	0.00
0.44	0.02	0.66	0.04	0.78	0.06	0.84	0.11
0.35	0.08	0.64	0.04	0.73	0.06	0.69	0.15
0.25	0.09	0.63	0.04	0.66	0.09	0.57	0.14
0.20	0.05	0.58	0.04	0.56	0.11	0.52	0.13
		0.52	0.04	0.50	0.11	0.48	0.11
		0.48	0.06	0.42	0.12	0.42	0.11
		0.44	0.06	0.38	0.13	0.40	0.11
		0.41	0.07	0.22	0.12	0.33	0.14
		0.36	0.09	0.13	0.08	0.25	0.14
		0.26	0.08	0.03	0.04	0.13	0.09
		0.25	0.08			0.11	0.08
		0.19	0.04			0.07	0.06
		0.16	0.03				

Table A.8 Results of Crack Sectioning

SPECIMEN B - 10

$R_\epsilon = 0$

$\Delta/2 = 1.0\%$

2c = 0.28		2c = 0.38		2c = 0.44		2c = 0.52	
L	a	L	a	L	a	L	a
0.28	0.00	0.38	0.00	0.44	0.00	0.52	0.00
0.28	0.01	0.33	0.06	0.31	0.07	0.48	0.01
0.26	0.01	0.23	0.06	0.27	0.07	0.39	0.06
0.13	0.07	0.14	0.03	0.15	0.09	0.29	0.08
0.02	0.02	0.07	0.02	0.11	0.06	0.19	0.09
		0.05	0.01	0.07	0.06	0.10	0.06
				0.05	0.06	0.03	0.06

2c = 0.59		2c = 0.63		2c = 0.84		2c = 1.19	
L	a	L	a	L	a	L	a
0.69	0.00	0.63	0.00	0.84	0.00	1.19	0.00
0.67	0.02	0.55	0.04	0.73	0.13	1.11	0.06
0.60	0.06	0.47	0.08	0.64	0.15	1.00	0.08
0.48	0.07	0.38	0.10	0.61	0.15	0.91	0.11
0.41	0.09	0.22	0.06	0.50	0.17	0.81	0.13
0.20	0.07	0.19	0.06	0.38	0.16	0.75	0.18
0.16	0.06	0.13	0.05	0.30	0.17	0.72	0.18
0.14	0.06			0.19	0.16	0.63	0.19
				0.17	0.16	0.53	0.21
						0.52	0.23
						0.44	0.23
						0.33	0.25
						0.14	0.20
						0.11	0.19

Table A.7 Results of Crack Sectioning

SPECIMEN B - 34

$R_\varepsilon = \overline{0}$

$\Delta/2 = 0.5\%$

2c = 0.19		2c = 0.28		2c = 0.39		2c = 0.52		2c = 0.61	
L	a	L	a	L	a	L	a	L	a
0.19	0.00	0.28	0.00	0.39	0.00	0.52	0.00	0.61	0.00
0.14	0.06	0.27	0.03	0.28	0.09	0.50	0.12	0.50	0.11
0.08	0.04	0.20	0.05	0.25	0.07	0.44	0.11	0.41	0.14
0.08	0.03	0.16	0.07	0.21	0.09	0.41	0.12	0.31	0.14
0.06	0.05	0.13	0.05	0.10	0.07	0.36	0.12	0.27	0.08
0.01	0.03	0.08	0.03	0.05	0.04	0.30	0.11	0.24	0.13
		0.03	0.03			0.08	0.07	0.06	0.04

2c = 0.69		2c = 0.84		2c = 0.94		2c = 1.16	
L	a	L	a	L	a	L	a
0.69	0.00	0.84	0.00	0.94	0.00	1.16	0.00
0.56	0.09	0.80	0.06	0.83	0.03	1.13	0.19
0.47	0.09	0.72	0.16	0.73	0.04	1.06	0.20
0.45	0.08	0.66	0.24	0.67	0.04	0.95	0.27
0.38	0.10	0.63	0.25	0.60	0.09	0.89	0.29
0.33	0.11	0.59	0.29	0.53	0.15	0.88	0.28
0.22	0.08	0.52	0.30	0.45	0.18	0.81	0.30
0.17	0.04	0.48	0.31	0.39	0.19	0.75	0.29
0.08	0.04	0.45	0.31	0.30	0.18	0.59	0.27
		0.42	0.32	0.23	0.18	0.50	0.27
		0.36	0.31	0.11	0.10	0.44	0.25
		0.23	0.32			0.38	0.22
		0.20	0.22			0.38	0.22
		0.16	0.18			0.31	0.14
		0.03	0.17				

Table A.9 Results of Crack Sectioning

SPECIMEN B - 12

$R_\varepsilon = -1$

$\Delta/2 = 0.5\%$

2c = 0.22		2c = 0.31		2c = 0.42		2c = 0.50	
L	a	L	a	L	a	L	a
0.22	0.00	0.31	0.00	0.42	0.00	0.50	0.00
0.16	0.04	0.30	0.06	0.38	0.06	0.42	0.16
0.13	0.04	0.25	0.12	0.19	0.09	0.34	0.16
0.09	0.08	0.19	0.11	0.11	0.11	0.27	0.11
0.05	0.05	0.16	0.14	0.09	0.11	0.20	0.11
0.02	0.03	0.09	0.13	0.03	0.03	0.09	0.11
		0.05	0.06				

2c = 0.59		2c = 0.75		2c = 0.91		2c = 1.03	
L	a	L	a	L	a	L	a
0.59	0.00	0.75	0.00	0.81	0.00	1.03	0.00
0.53	0.14	0.56	0.28	0.84	0.20	0.84	0.06
0.48	0.11	0.53	0.30	0.72	0.24	0.73	0.20
0.39	0.09	0.34	0.34	0.67	0.25	0.64	0.30
0.30	0.09	0.30	0.33	0.61	0.29	0.56	0.30
0.22	0.16	0.28	0.30	0.47	0.31	0.48	0.33
0.12	0.17	0.22	0.28	0.38	0.33	0.39	0.30
		0.17	0.24	0.31	0.32	0.34	0.31
		0.14	0.14	0.19	0.28	0.28	0.39
		0.08	0.10	0.10	0.27	0.16	0.42
						0.08	0.16

Table A.10 Results of Crack Sectioning

SPECIMEN B - 15

R_ε - 0

$\Delta/2$ = 0.5%

2c = 0.19		2c = 0.38		2c = 0.52		2c = 0.58	
L	a	L	a	L	a	L	a
0.19	0.00	0.38	0.00	0.52	0.00	0.58	0.00
0.16	0.05	0.28	0.12	0.47	0.08	0.52	0.13
0.13	0.06	0.22	0.13	0.45	0.09	0.42	0.17
0.09	0.09	0.09	0.08	0.42	0.14	0.38	0.14
0.07	0.09	0.05	0.08	0.34	0.08	0.36	0.16
0.03	0.04	0.03	0.06	0.22	0.13	0.31	0.13
				0.19	0.11	0.16	0.16
				0.11	0.05	0.09	0.11

2c = 0.68		2c = 0.72		2c = 0.81		2c = 0.97	
L	a	L	a	L	a	L	a
0.68	0.00	0.72	0.00	0.81	0.00	0.97	0.00
0.67	0.11	0.66	0.01	0.77	0.18	0.84	0.13
0.66	0.16	0.61	0.08	0.69	0.18	0.77	0.13
0.63	0.14	0.53	0.10	0.66	0.20	0.75	0.14
0.59	0.11	0.47	0.14	0.53	0.22	0.70	0.16
0.50	0.08	0.39	0.15	0.48	0.18	0.63	0.15
0.47	0.06	0.28	0.06	0.41	0.17	0.53	0.13
0.44	0.07			0.33	0.06	0.50	0.13
0.39	0.11			0.28	0.17	0.38	0.19
0.34	0.13			0.19	0.13	0.28	0.23
0.30	0.14			0.16	0.13	0.25	0.25
0.19	0.13			0.14	0.12	0.22	0.24
0.11	0.16			0.08	0.11	0.20	0.22
						0.17	0.23
						0.09	0.19

6. REFERENCES

1. Garud, Y. S., "Multiaxial Fatigue: A Survey of the State of the Art," JTEVA, Vol. 9, 1981, pp. 165-178.

2. Brown, M. W., and K. J. Miller, "Low Cycle Fatigue and Life Prediction," ASTM STP 770, 1982, pp. 482-499.

3. Brown, M. W., and K. J. Miller, "A Theory for Fatigue under Multiaxial Stress-Strain Conditions," Proc., Inst. Mech. Engrs., 187 (1973), pp. 745-755.

4. Lohr, R. D., and E. G. Ellison, "A Simple Theory for Low Cycle Multiaxial Fatigue," Fatigue Engr. Mat. Struct., 3, 1980, pp. 1-17.

5. Socie, D. F., L. A. Waill, D. F. Dittmer, "Biaxial Fatigue of Inconel 718 including Mean Stress Effect," ASTM STP, Biaxial/ Multiaxial Fatigue.

6. Waill, L. E., "Crack Observations in Biaxial Fatigue," Master of Science Thesis, Dept. of Mech. and Ind. Eng., University of Illinois at U-C., 1983, Report No. 108.

7. Forsyth, P.J.E., "A Two-Stage Process of Fatigue Crack Growth," Proc., Crack Propagation Symp., Cranfield (1961), pp. 76-94.

8. Dowling, N. E., "Growth of Short Fatigue Cracks in an Alloy Steel," Westinghouse Research Laboratories, Scientific Paper 82-1D7-STINE-P1, Pittsburgh, Pa., 1982.

9. Irving, P. E., "Microcrack Growth and Torsional Fatigue," GKN Technology, Ltd., Birmingham New Road, Wolverhampton, England, WV4 6BW.